Computational Issues in Oil Field Applications :

Methodologies and Robust Algorithms for Subsurface Simulators

Workshop I:

Multiphysics, Multiscale, and Coupled Problems in Subsurface Physics

Mary F. Wheeler

CENTER FOR SUBSURFACE MODELING

The University of Texas at Austin

Acknowledge

Collaborators

Ben Ganis	Gergina Pencheva
Gurpreet Singh	Sanghyun Lee
Thomas Wick	Andro Mikelic
Baehyun Min	Deandre White
Mohammad Beygi	Mohammad Lotfollahi
Sogo Shiozawa	Mohammad Jammoul

Research Initiative: Closed-loop Workflow

I. FLUID-DRIVEN FRACTURE PROPAGATION

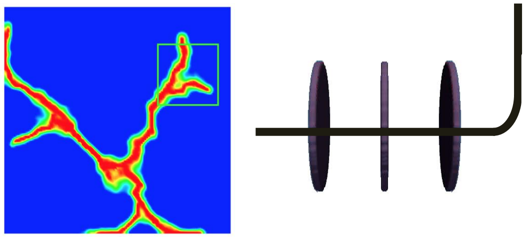

IV. UNCERTAINTY QUANTIFICATION

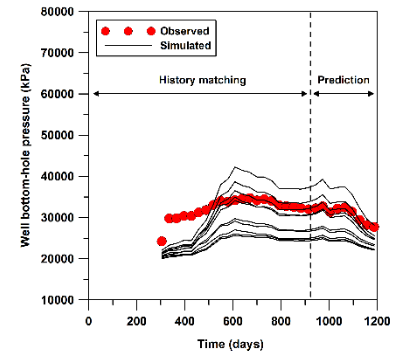

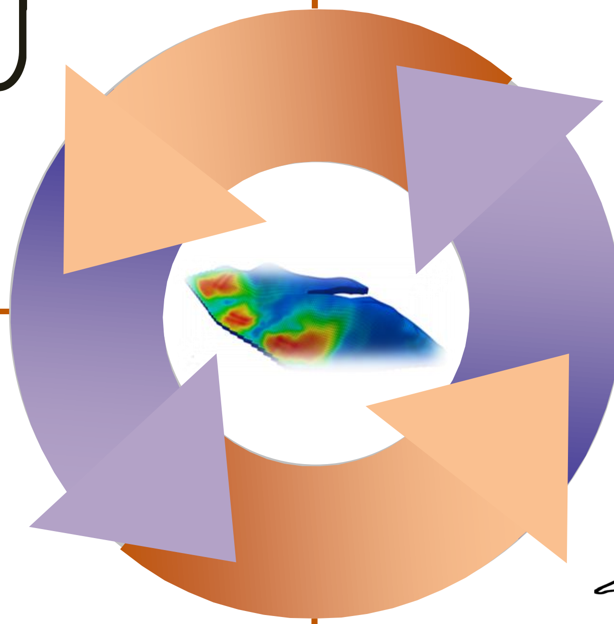

II. PHASE & CHEMICAL EQUILIBRIUM

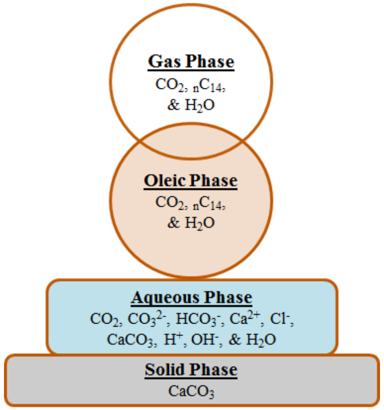

III. SIMULATOR DEVELOPMENT

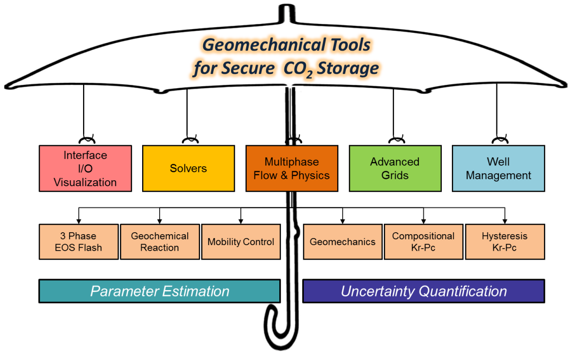

V. BIG DATA: Cross-cutting Initiative

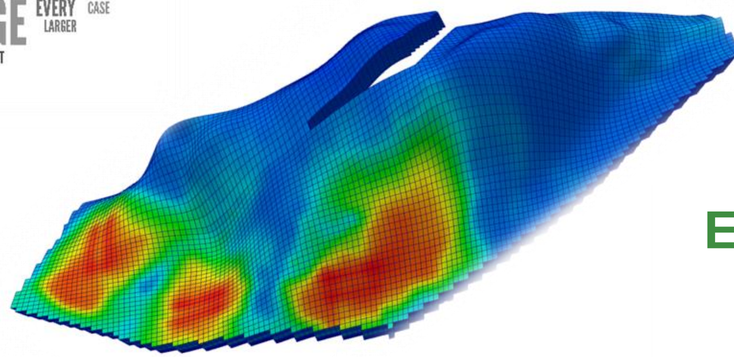

Exascale Computing

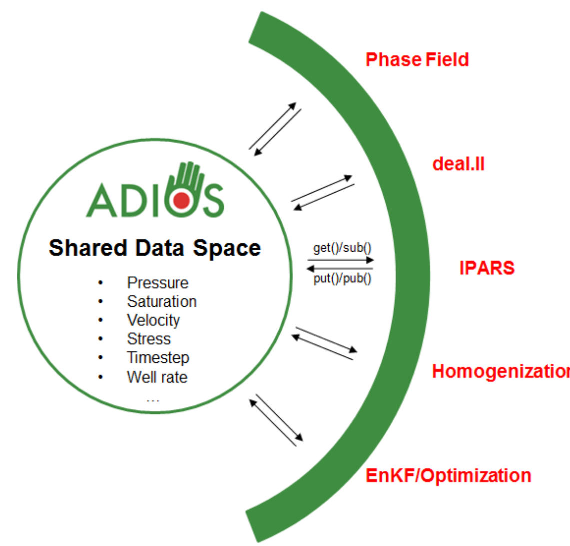

I. FLUID-DRIVEN FRACTURE PROPAGATION

Objectives

Develop a **fracture propagation** method (phase field) driven by multiphysics, multiphase fluid flow

- Three dimensional computations using **mesh adaptivity** with coupling displacements, **phase field**, and pressure system
- In the phase field fracture propagation model, **primal-dual active set & fixed-stress** iteration is coupled to solve the whole system
- Demonstrate the potential of the phase field for treating practical engineering applications by providing numerical examples

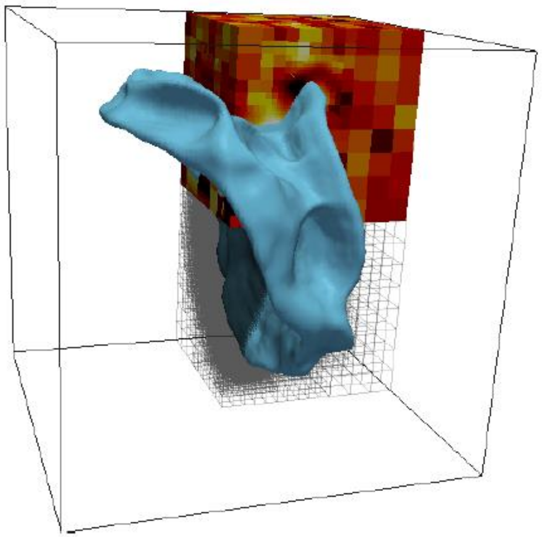

Joining and branching of non-planar hydraulic fractures in 3D heterogeneous media.

Advantage of Phase Field Model

- Classical theory of crack propagation [Griffith 1921]
- Diffusive crack zones for free discontinuity problems
- Γ-Convergent approximation [Ambrosio-Tortorelli 1992]
- Variational methods based on energy minimization

  [Francfort-Marigo 2003], [Miehe et al. 2010]

Variation methods based energy minimization

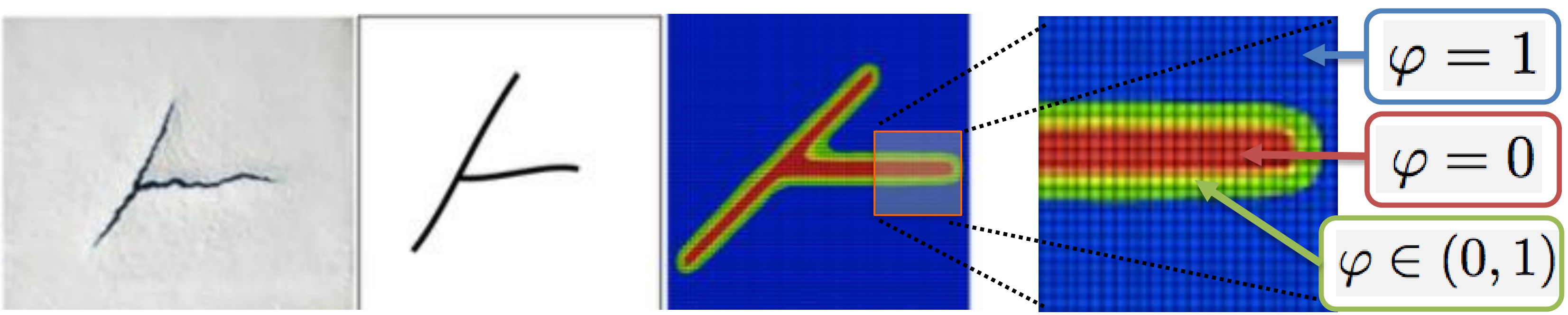

[Real fractures] [Interface approach] [Diffusive approach using Phase field]

Advantage of Phase Field Model

- Fixed-topology approach **avoiding re-meshing**
- Determine **crack nucleation, propagation, and the path** automatically
- Simple to handle **joining and branching** of (multiple) cracks
- Promising findings for future ideas as an indicator function

  based on theory and numerical simulations

Before joining	After joining	Branching
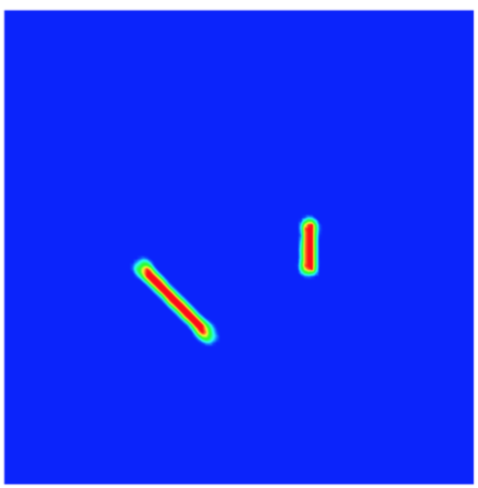	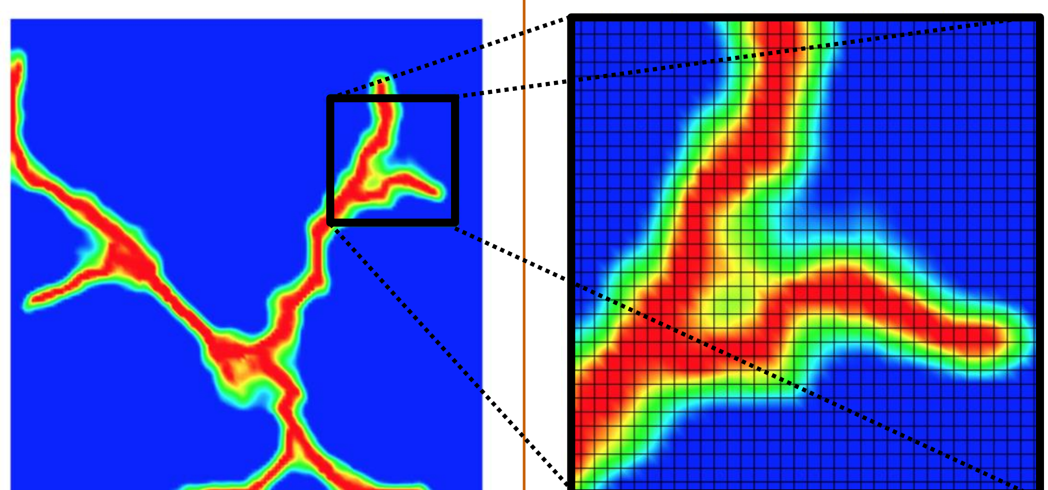	

Governing System: Biot's System

Biot's system

- Pressure Diffraction System

$$\rho_R \partial_t (\frac{1}{M} p_R + \alpha \nabla \cdot \mathbf{u}) - \nabla \cdot \frac{K_R \rho_R}{\eta_R} (\nabla p_R - \rho_R \mathbf{g}) = q_R \quad \text{in} \quad \Omega_R(t) \times (0,T]$$

$$\rho_F \partial_t (c_F p_F) - \nabla \cdot \frac{K_F \rho_F}{\eta_F} (\nabla p_F - \rho_F \mathbf{g}) = q_F - q_L \quad \text{in} \quad \Omega_F(t) \times (0,T]$$

$$[p_j] = 0 \quad \text{on} \quad \Gamma(t) \times (0,T]$$

$$[K_j (\nabla p_j - \rho_j \mathbf{g})] \cdot \mathbf{n} = 0 \quad \text{on} \quad \Gamma(t) \times (0,T]$$

[Mikelic-W.-Wick 2015 SIAM MMS]

- Mechanics and Phase Field

$$E_\varepsilon(\mathbf{u}, p, \varphi) = \int_\Lambda \frac{1}{2}((1-k)\varphi^2 + k)\mathcal{G}e(\mathbf{u}) : e(\mathbf{u})\, dx - \int_{\partial\Lambda} \tau \cdot \mathbf{u}\, dS$$

$$- \int_\Lambda (\alpha - 1)\varphi^2 p \operatorname{div} \mathbf{u}\, dx + \int_\Lambda (\varphi^2 \nabla p)\mathbf{u}\, dx + G_c \int_\Lambda \left(\frac{1}{2\varepsilon}(1-\varphi^2) + \frac{\varepsilon}{2} |\nabla \varphi^2| \right) dx$$

- Linear Elasticity
- Newton Iteration
- Primal-dual Active Set Method

[Heister-W.Wick 2015 CMAME]

Fracture with maximum pressure

- The pressure starts to decrease when the fracture starts to propagate.

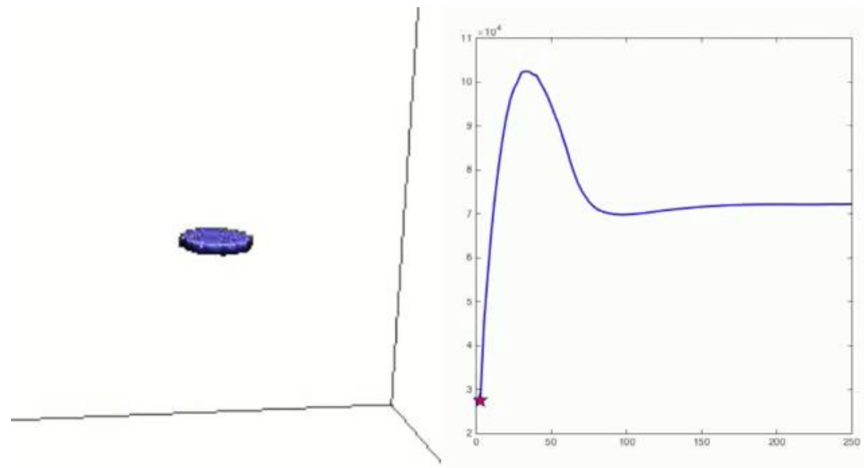

(a) Phase Field (b) Pressure

[Lee-W.-Wick 2016 CMAME]

Numerical Examples of Phase Field

Multiple fractures propagating near wellbore [Lee-W.-Wick 2016]

- Fracture propagation

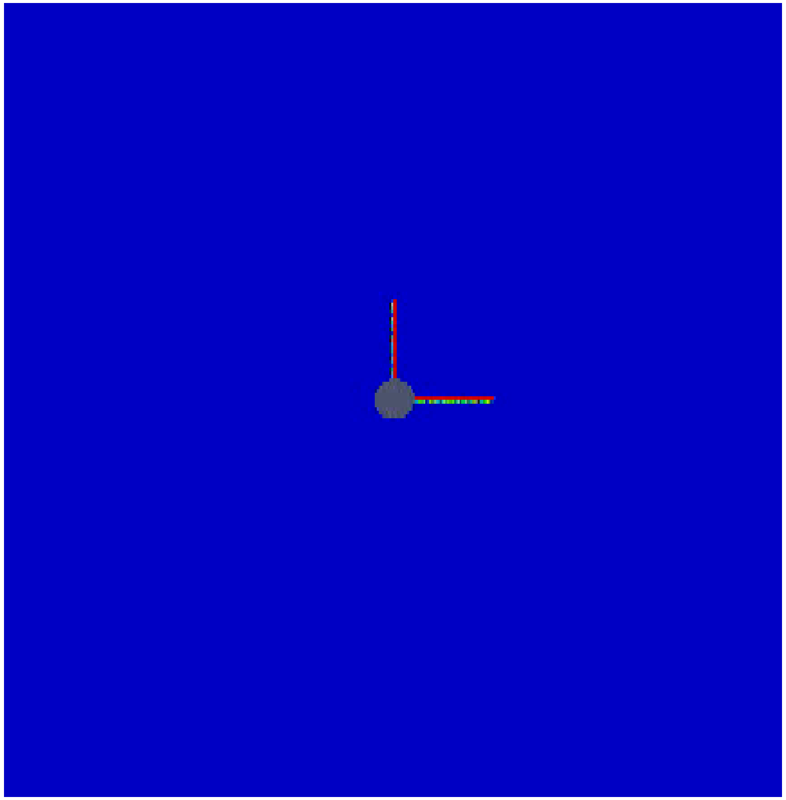

- Pressure distribution

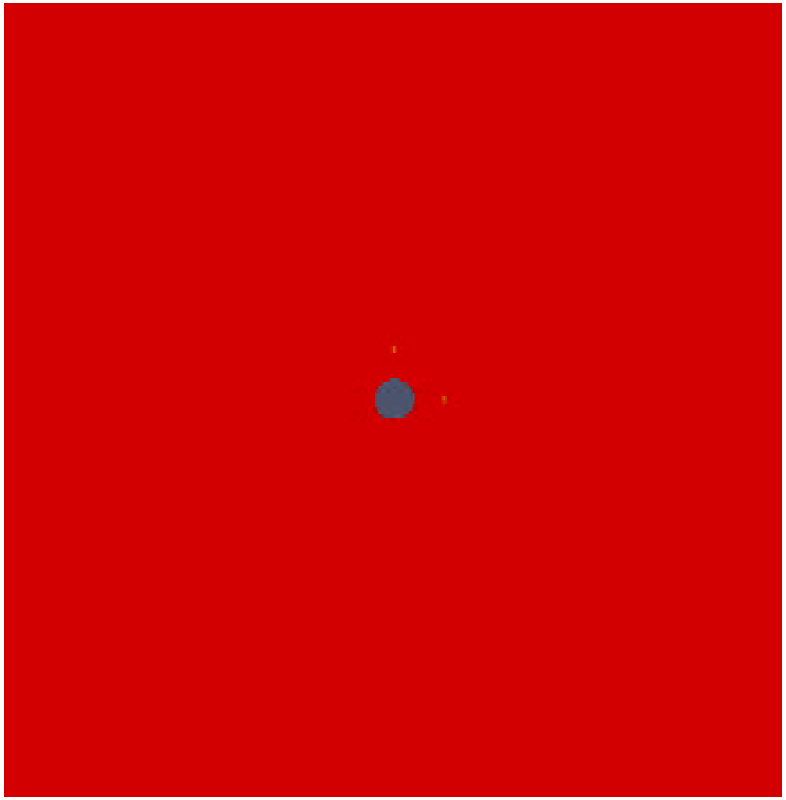

Numerical Examples of Phase Field

Three parallel fractures in 3D domain [Lee-W.-Wick 2016]

- Not all fractures are growing due to stress-shadowed effects.

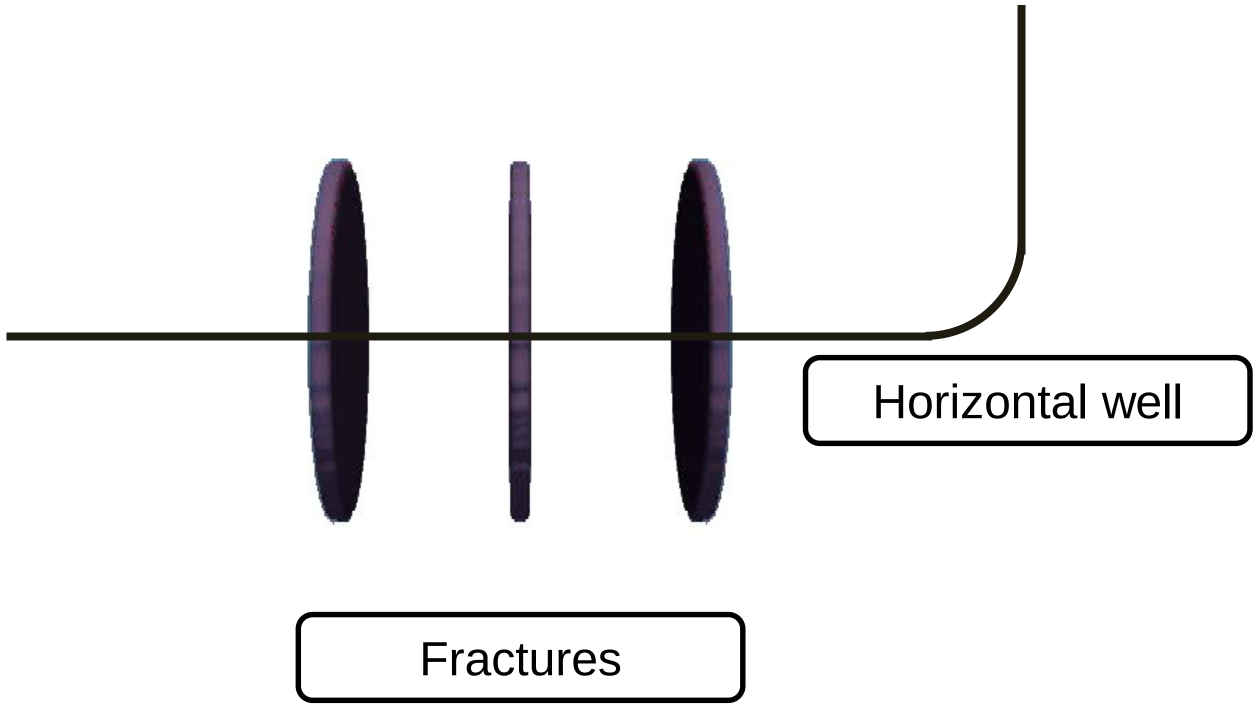

Numerical Examples of Phase Field

Multiple fractures in a 3D heterogeneous medium [Lee-W.-Wick 2015]

- Dynamic mesh adaptivity: predictor-corrector method [Heister-Wheeler-Wick, 2015]

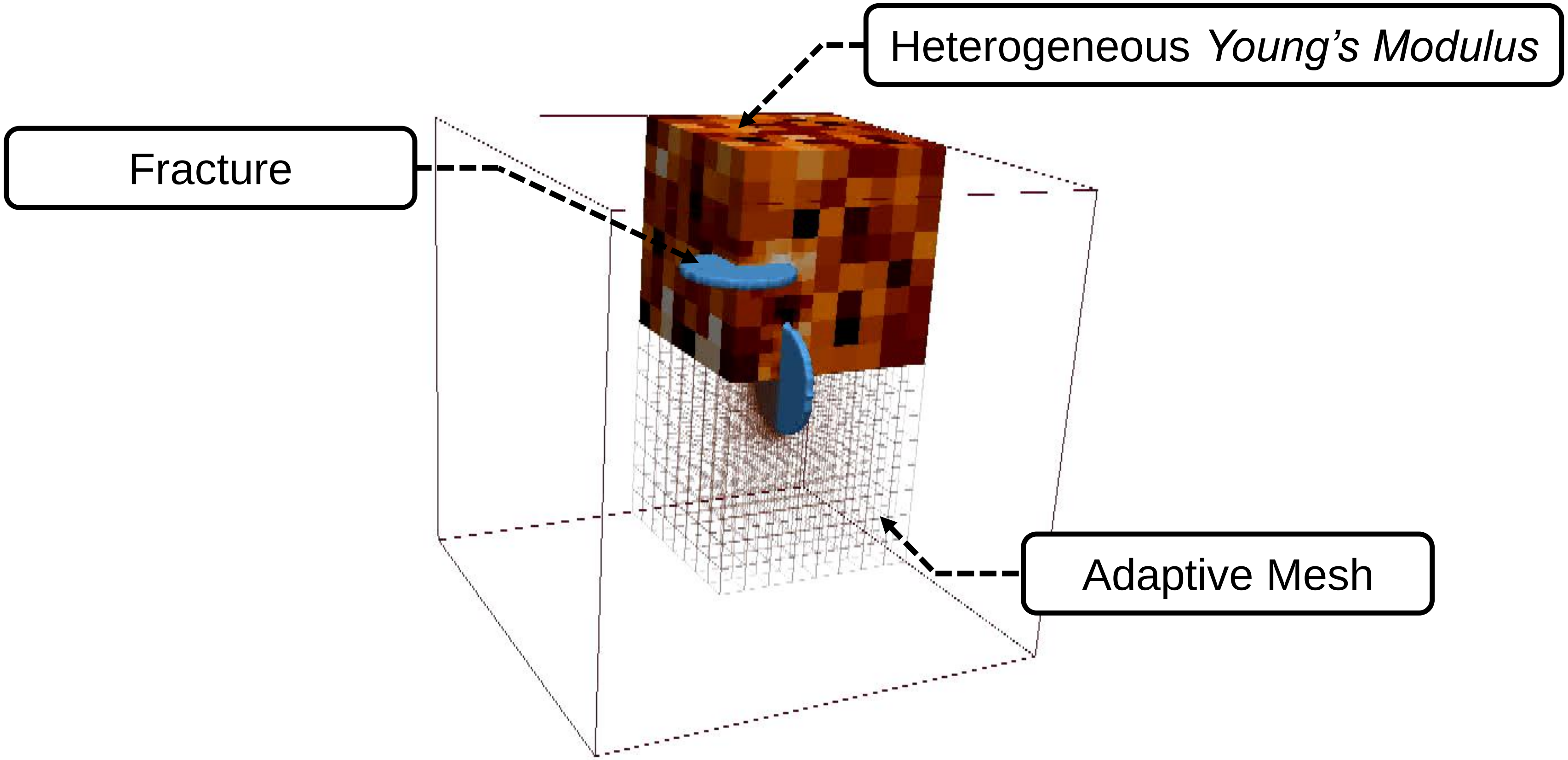

II. GEOCHEMICAL REACTIONS

Objectives

Model geochemical reactions of injected CO_2 in carbonate reservoirs during EOR or CO_2 sequestration

- In situ brines with reactive ionic species
- Study the effect of reactive species on CO_2 concentration
- Quantify the effect using changes in miscibility conditions during CO_2 EOR

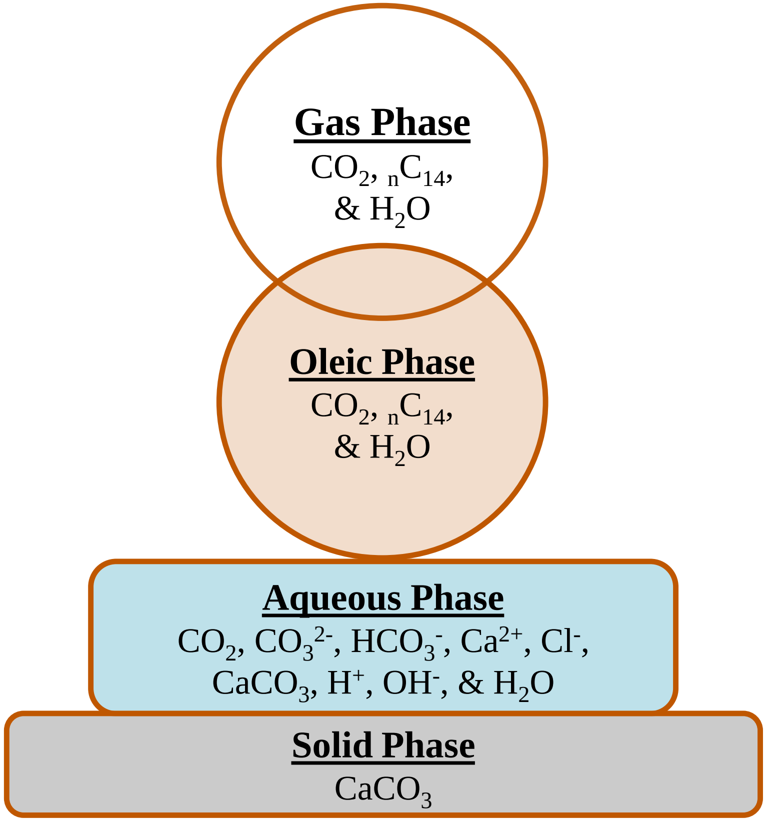

[Phase & Chemical Equilibrium of CO_2]

Coupling with a Compositional Simulator

Coupled phase and chemical equilibrium

- Gibbs Free Energy Minimization

Reactions ⟷ **Phase behavior**

Gibbs free energy minimization

Stochiometric approach

- Equation of State (EOS)

$$\frac{\partial}{\partial t}\left(\sum_{j}^{N_p}\phi S_j \rho_j x_{ij}\right)+\nabla\cdot\sum_{j}^{N_p}\left(\rho_j x_{ij} u_j-\phi S_j D_{ij}\cdot\nabla\left(\rho_j x_{ij}\right)\right)=\sum_{j}^{N_p}\left(q_{ij}+\boxed{r_{ij}}\right)$$

$$u_j=-K\frac{k_{rj}}{\mu_j}\left(\nabla p_j-\rho_{m,j}g\right)$$

where r_{ij} : rate of change of component i in phase j due to chemical equilibrium

(r_{ij} = 0 if no reaction)

Example: Effect of Reactions on CO_2 Concentration

Concentration profiles at P_{avg} = 2,200 psi after 0.12 hours of CO_2 injection

- Red curve ( ): concentration profiles with equilibrium reactions
- Black curve ( ): concentration profiles without equilibrium reactions
- Reactions in aqueous phase consume CO_2 altering phase equilibrium and hence miscibility conditions.
- Higher in situ water saturation results in lower CO_2 concentrations.

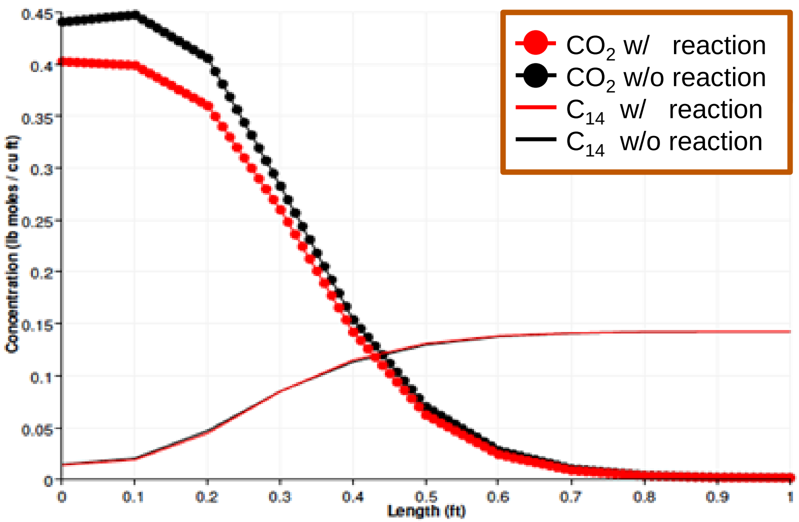

Sw = 0.3

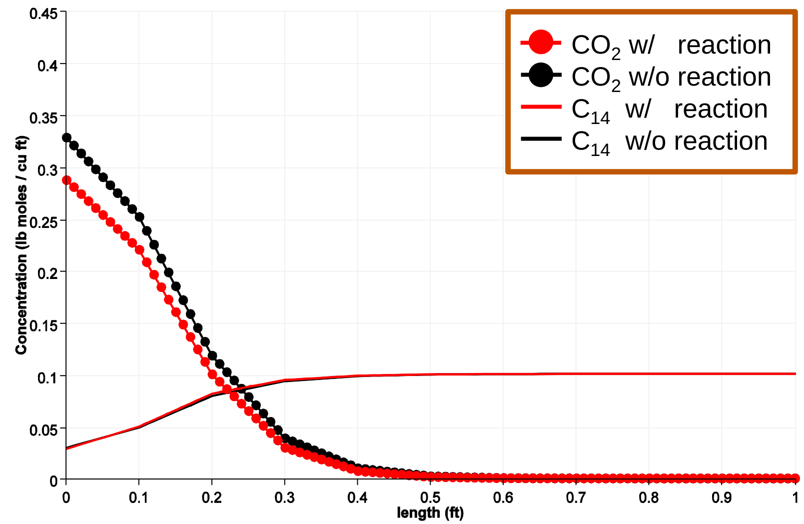

Sw = 0.5

Locally Conservative Flow and Transport- Enhanced Galerkin

Transport Equation

$$\partial_t(\rho\phi c) + \nabla\cdot(\rho\mathbf{u}\mathbf{c} - \mathbf{D}(\mathbf{u})\nabla\mathbf{c}) = \mathbf{c}^*\mathbf{q}^*$$

- Inflow and outflow boundary conditions.
- Initial condition : $c(x,0) = c_0(x) \quad \forall x \in \Omega$.
- $\rho(p) \sim \rho_0(1 + c_F p)$, and $\varepsilon \equiv 0$
- c^+, q^+: source term, c^-, q^-: sink term.

Locally Conservative Flux : Weighted Interior Penalty (Ern et al., 2007)

$$\begin{aligned}
\mathbf{U}^n|_T &= -\boldsymbol{\kappa}\nabla P^n, \quad \forall T \in \mathcal{T}_h \\
\mathbf{U}^n\cdot\mathbf{n}|_e &= -\boldsymbol{\kappa}_e\{\!\{\nabla P^n\}\!\}\cdot\mathbf{n} + \alpha(k)h_e^{-1}\boldsymbol{\kappa}_e[\![P^n]\!], \quad \forall e \in \mathcal{E}_h^o, \\
\mathbf{U}^n\cdot\mathbf{n}|_e &= g_N, \quad \forall e \in \mathcal{E}_h^{N,\partial}, \\
\mathbf{U}^n\cdot\mathbf{n}|_e &= -\boldsymbol{\kappa}\nabla P^n\cdot\mathbf{n} + \alpha(k)h_e^{-1}\boldsymbol{\kappa}\left(P^n - g_D\right), \quad \forall e \in \mathcal{E}_h^{D,\partial},
\end{aligned}$$

$$\boldsymbol{\kappa}_e\{\!\{\nabla v\}\!\} = \beta_e(\boldsymbol{\kappa}^+(\nabla v)^+) + (1-\beta_e)(\boldsymbol{\kappa}^-(\nabla v)^-)$$

$$\beta_e := \frac{\boldsymbol{\kappa}^-}{\boldsymbol{\kappa}^+ + \boldsymbol{\kappa}^-} \qquad \boldsymbol{\kappa}_e := \frac{2\boldsymbol{\kappa}^+\boldsymbol{\kappa}^-}{\boldsymbol{\kappa}^+ + \boldsymbol{\kappa}^-}$$

- $\boldsymbol{\kappa} = \frac{K}{\mu}$, $\boldsymbol{\kappa}_e$: Harmonic mean on the edge
- α, k : coefficients for the penalty term

Locally Conservative Flow and Transport- Enhanced Galerkin

- **EG Transport – Entropy residual stabilization** [Guermond et al. 08, 11]

Concentration values over the time steps (observe spurious oscillations)

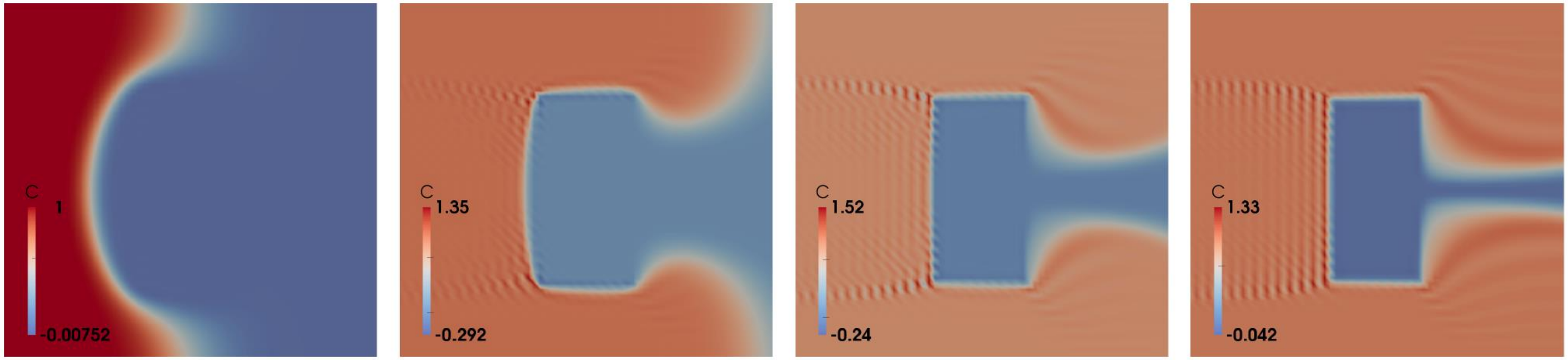

(a) n=50 (b) n=100 (c) n=150 (d) n=200

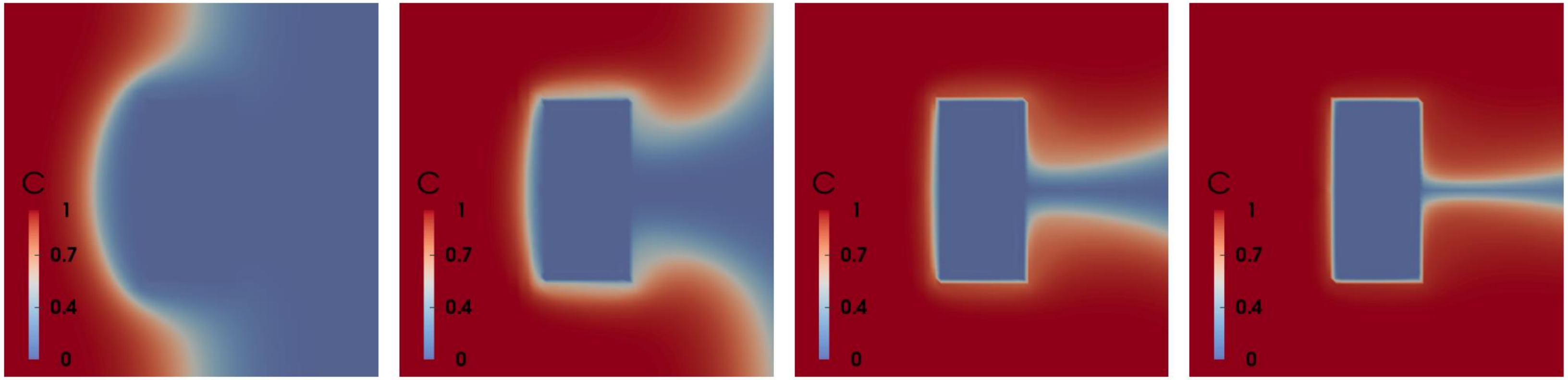

(e) n=50 (f) n=100 (g) n=150 (h) n=200

Miscible two components single phase flow

Hele-Shaw cell: viscous fingering in a homogeneous channel [Lee-W. 2016]

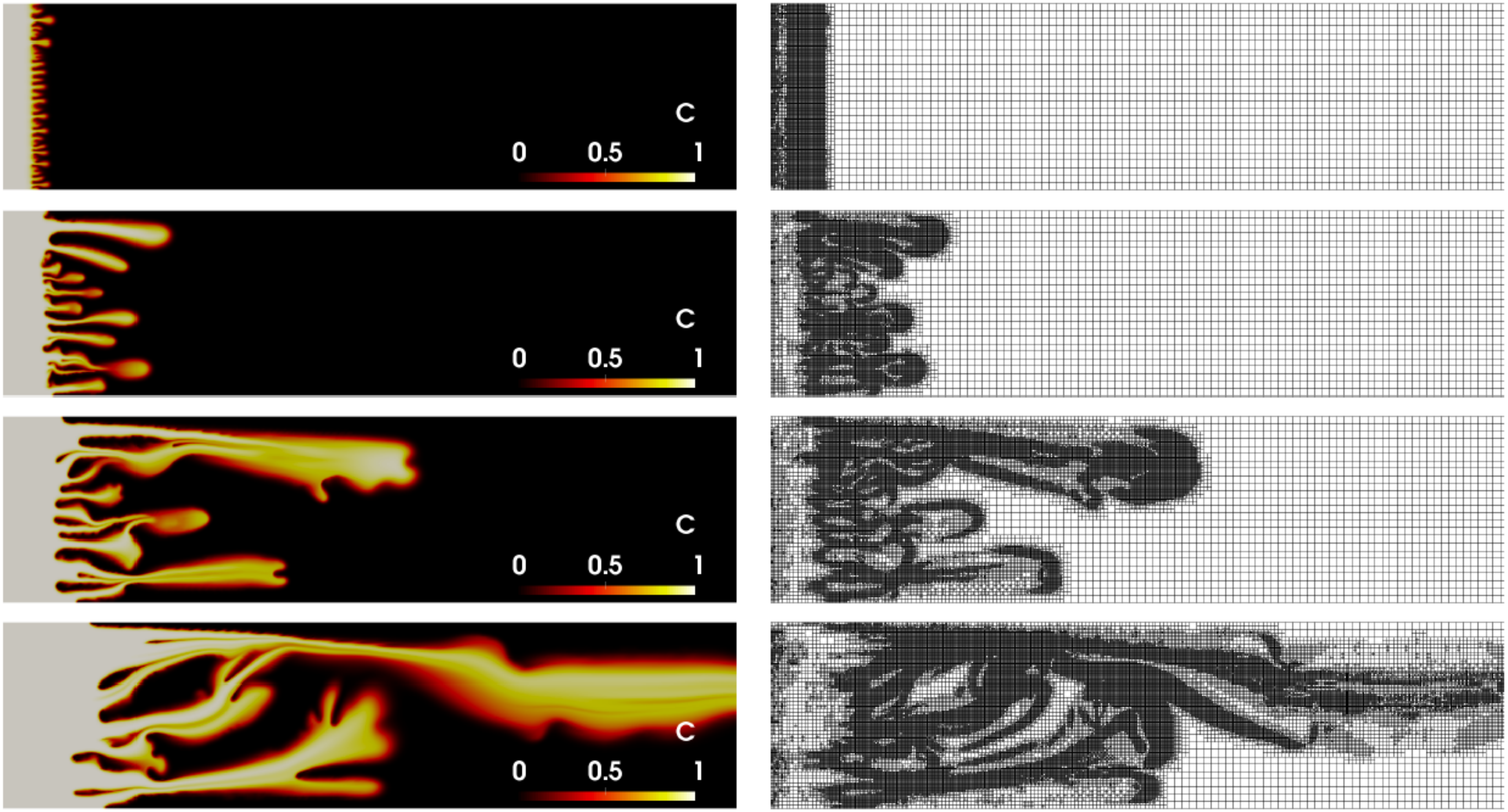

Figure: Concentration values for each time steps with corresponding adaptive mesh refinement at the right column.

III. SIMULATOR DEVELOPMENT

Objectives

Complete simulator development with numerical schemes for coupled processes

- Develop computational methods for coupled processes based on multiscale discretization for **flow, geomechanics & geochemistry**
- Development of efficient **solvers & pre-conditioners**
- **Model CO_2 storage field sites** & perform compositional simulations

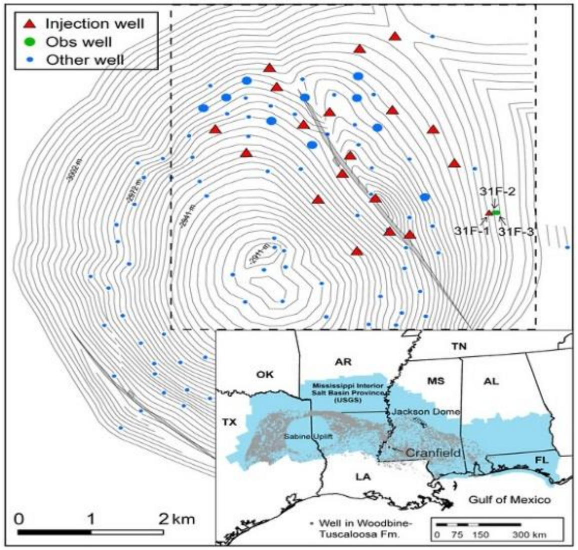

CO_2 Sequestration Site at Cranfield, Mississippi, USA

Framework of IPARS

- **IPARS** (**I**ntegrated **P**arallel **A**ccurate **R**eservoir **S**imulator)

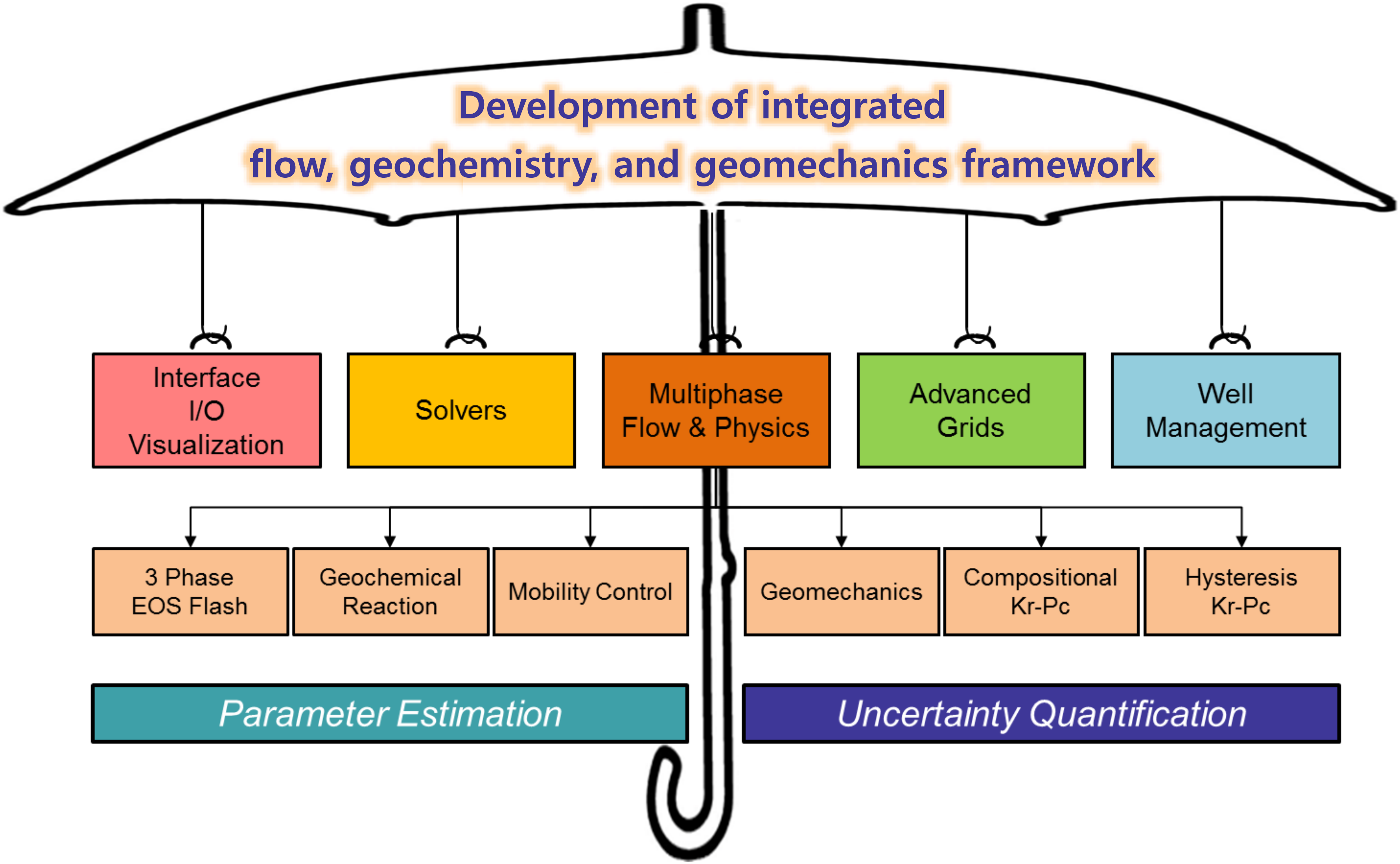

Compositional Model

3-Phases: $\alpha \in \{o, w, g\}$ N_c-Components: $i \in \{w, 2, \ldots, N_c\}$

Mass Conservation of component i:

$$\frac{\partial}{\partial t}\left(\sum_{\alpha} \phi S_\alpha \rho_\alpha \xi_{i\alpha}\right) + \nabla \cdot \sum_{\alpha} \left(\rho_\alpha \xi_{i\alpha} u_\alpha - \phi S_\alpha D_{i\alpha} \cdot \nabla \left(\rho_\alpha \xi_{i\alpha}\right)\right) = \sum_{\alpha} q_{i\alpha}, \quad \text{in } \Omega \times (0, T].$$

Darcy's Law for phase α flux: $u_\alpha = -K \frac{k_{r\alpha}}{\mu_\alpha} \left(\nabla p_\alpha - \rho_{m,\alpha} g\right).$

S_α	saturation	$\xi_{i\alpha}$	mole fraction	μ_α	viscosity
ϕ	porosity	K	absolute permeability	$\rho_{m,\alpha}$	mass density
$q_{i\alpha}$	source/sink	$k_{r\alpha}$	relative permeability	g	gravity
u_α	Darcy flux	$D_{i\alpha}$	diffusion-dispersion		

Concise Form of Equations

Concentration of component i
$$N_i = \sum_{\alpha} \rho_\alpha S_\alpha \xi_{i\alpha},$$

Source of component i
$$q_i = \sum_{\alpha} q_{i\alpha},$$

Advective flux of component i
$$F_i = -K \sum_{\alpha} \rho_\alpha \xi_{i\alpha} \frac{k_{r\alpha}}{\mu_\alpha} \left(\nabla p_\alpha - \rho_{m,\alpha} g\right),$$

Diffusive flux of component i
$$J_i = -\left(\sum_{\alpha} \phi S_\alpha D_{i\alpha} \left(\nabla \rho_\alpha \xi_{i\alpha}\right)\right).$$

Concise form of component concentration equation:
$$\frac{\partial}{\partial t}(\phi N_i) + \nabla \cdot (F_i + J_i) = q_i, \quad \text{in } \Omega \times (0, T].$$

Constraints, Initial, and Boundary Conditions

Primary model unknowns $p_{ref}, N_1, \ldots, N_{N_c}$

Saturation constraint $\sum_{\alpha} S_{\alpha} = 1 \Rightarrow \frac{N_w}{\rho_w} + \left(\frac{1-\nu}{\rho_o} + \frac{\nu}{\rho_g}\right) \sum_{i=2}^{N_c} N_i = 1$

Capillary pressure $p_{c\alpha}(S_{ref}) = p_{\alpha} - p_{\text{ref}} \Rightarrow p_{c\alpha}(p_{ref}, \vec{N}) = p_{c\alpha}(S_{ref})$

Slightly compressible for water phase $\rho_w(p_{ref}) = \rho_{w,0} exp\left[C_w(p_{\text{ref}} + p_{cw} - p_{\text{ref},0})\right]$

Cubic EOS for hydrocarbon phases $\rho_{\alpha}(p_{ref}, \vec{N}_{HC}) = \frac{p_{\alpha}}{Z_{\alpha} RT}, \alpha \neq \mathrm{w}$

No-flow boundary conditions $(F_i + J_i) \cdot n = 0, \quad \text{on } \partial\Omega \times [0, T]$

Initial conditions $p_{\text{ref}} = p^0, \quad N_i = N_i^0, \quad \text{on } \Omega \times \{t = 0\}$

Hydrocarbon Phase Behavior Model

Peng-Robinson Equation of State

(for compressibility Z-factor; coefficients determin ed by pressure, temperature, composition)

$$Z_\alpha = \overline{Z}_\alpha - C_\alpha$$
$$\overline{Z}_\alpha^3 + h_1 \overline{Z}_\alpha^2 + h_2 \overline{Z}_\alpha + h_3 = 0 \qquad (1)$$

Rachford-Rice Equation

(for vapor fraction v)

$$\mathscr{R}_g = \sum_i \frac{(k_i - 1) z_i}{1 + (k_i - 1) v} = 0 \qquad (2)$$

"Mixing Rule"

(for mass balance)

$$\xi_i^o = \frac{z_i}{1 + (k_i - 1) v}, \quad \xi_i^g = k_i \xi_i^g \qquad (3)$$

Fugacity Coefficient Equation

f_i^α = fugacity $\Phi_i^\alpha = f_i^\alpha / (\xi_i^\alpha p)$ = fugacity coefficient

$$f_i^g = f_i^g$$
$$\mathscr{R}_i = ln(\Phi_i^o) - ln(\Phi_i^g) - ln(k_i) = 0 \qquad (4)$$

<u>Flash Algorithm</u> (Solved with Newton iteration)

1. Solve (2) for v .
2. Evaluate ξ_i^α using (3).
3. Solve (1) for Z_α.
4. Evaluate Φ_i^α, check (4) for convergence. Update $\delta(ln\, k_i)$, goto 1.

Multipoint Flux Mixed Finite Elements

- Multipoint Flux Mixed Finite Element Spaces

2D quadrilaterals 3D hexahedra

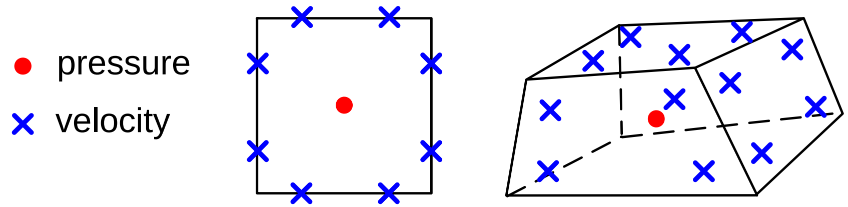

2 fluxes/edge 4 fluxes/face

- Special Quadrature Rules

$$K^{-1}(\hat{x}) = \frac{1}{J_E} DF_E^T K^{-1}(F_E(\hat{x})) DF_E .$$

$$(K^{-1}q, v)_{Q,E} = (K^{-1}\hat{q}, \hat{v})_{\hat{Q},\hat{E}} \equiv \frac{|\hat{E}|}{n_v} \sum_{i=1}^{n_v} K^{-1}(\hat{r}_i)\hat{q}(\hat{r}_i) \cdot \hat{v}(\hat{r}_i),$$

  – At every vertex, 12 flux DOFs eliminated in terms of 8 pressure DOFs.

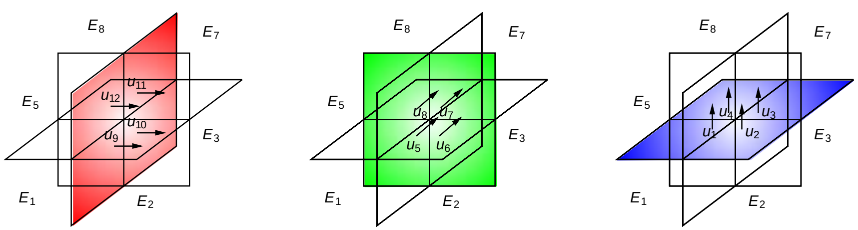

- Logically structured distorted hexahedral grids

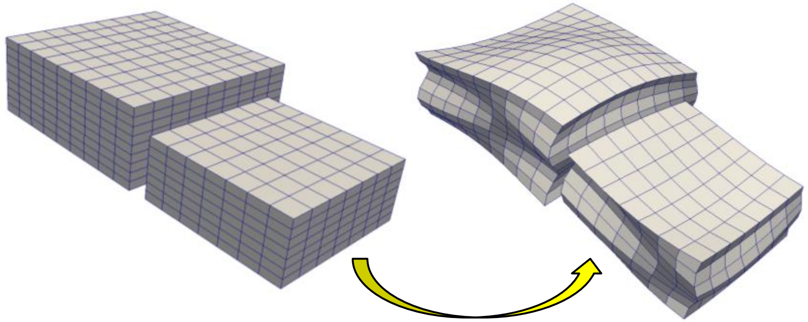

- No saddle point system with a mixed method.
  – 27-point stencil
  – Positive definite linear system
  – Symmetric or non-symmetric

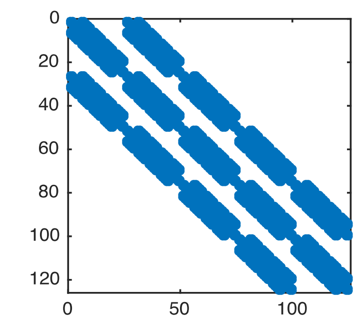

Matrix sparsity, 5x5x5 grid.

- Other capabilities:
  – Can handle full tensor permeability.
  – Finite element convergence theory.
  – Two-point flux schemes are not conv ergent on distorted hexahedra.

Fully Discrete Formulation

Component Flux:

$$\left\langle \frac{1}{\Lambda_{i,h}^{\tilde{k}}} \boldsymbol{K}^{-1} \boldsymbol{F}_{i,h}^{k+1}, v_h \right\rangle_{Q,E} - \left(p_{\mathrm{ref},h}^{k+1}, \nabla \cdot v_h \right)_E = -\int_{\partial E \cap \partial \Omega} p_{\mathrm{ref}} v_h \cdot n - \left(\frac{1}{\Lambda_{i,h}^{\tilde{k}}} \sum_{\alpha \neq \mathrm{ref}} \rho_{\alpha,h}^{\tilde{k}} \xi_{i\alpha,h}^{\tilde{k}} \lambda_{\alpha,h}^{\tilde{k}} \nabla p_{c\alpha,h}^{\tilde{k}}, v_h \right)_E$$
$$+ \left(\frac{1}{\Lambda_{i,h}^{\tilde{k}}} \sum_{\alpha} \left(\rho_{\alpha,h}^2 \right)^{\tilde{k}} \xi_{i\alpha,h}^{\tilde{k}} g, v_h \right)_E ,$$

Component Conservation Equation:

$$\left(\frac{\phi_h^{k+1} N_{i,h}^k}{\Delta t}, w_h \right)_E + \left(\nabla \cdot \boldsymbol{F}_{i,h}^{k+1}, w_h \right)_E - \left(\nabla \cdot \sum_{\alpha} \left\{ \phi_h^{k+1} S_{\alpha,h}^{\tilde{k}} \boldsymbol{D}_{i\alpha,h} \cdot \nabla \left(\rho_{\alpha,h}^{\tilde{k}} \xi_{i\alpha,h}^{\tilde{k}} \right) \right\}, w_h \right)_E$$
$$= \left(q_{i,h}^{\tilde{k}}, w_h \right) + \left(\frac{\phi^n N_i^n}{\Delta t}, w_h \right)_E .$$

- Solved with IMPEC scheme, iterative coupling
- Enhanced $BDDF_1$ mixed finite element space
- Symmetric and non-symmetric quadrature rules (Q)
- Λ_i's are positive quantities

Ex: Strong Scaling, Hard Phase Behavior

- Initial reservoir composition: {C3=0.1, C6=0.3, C10=0.1, C15=0.1, C20=0.4}
- Gas injection well composition: {C1=0.99, C3=0.01}

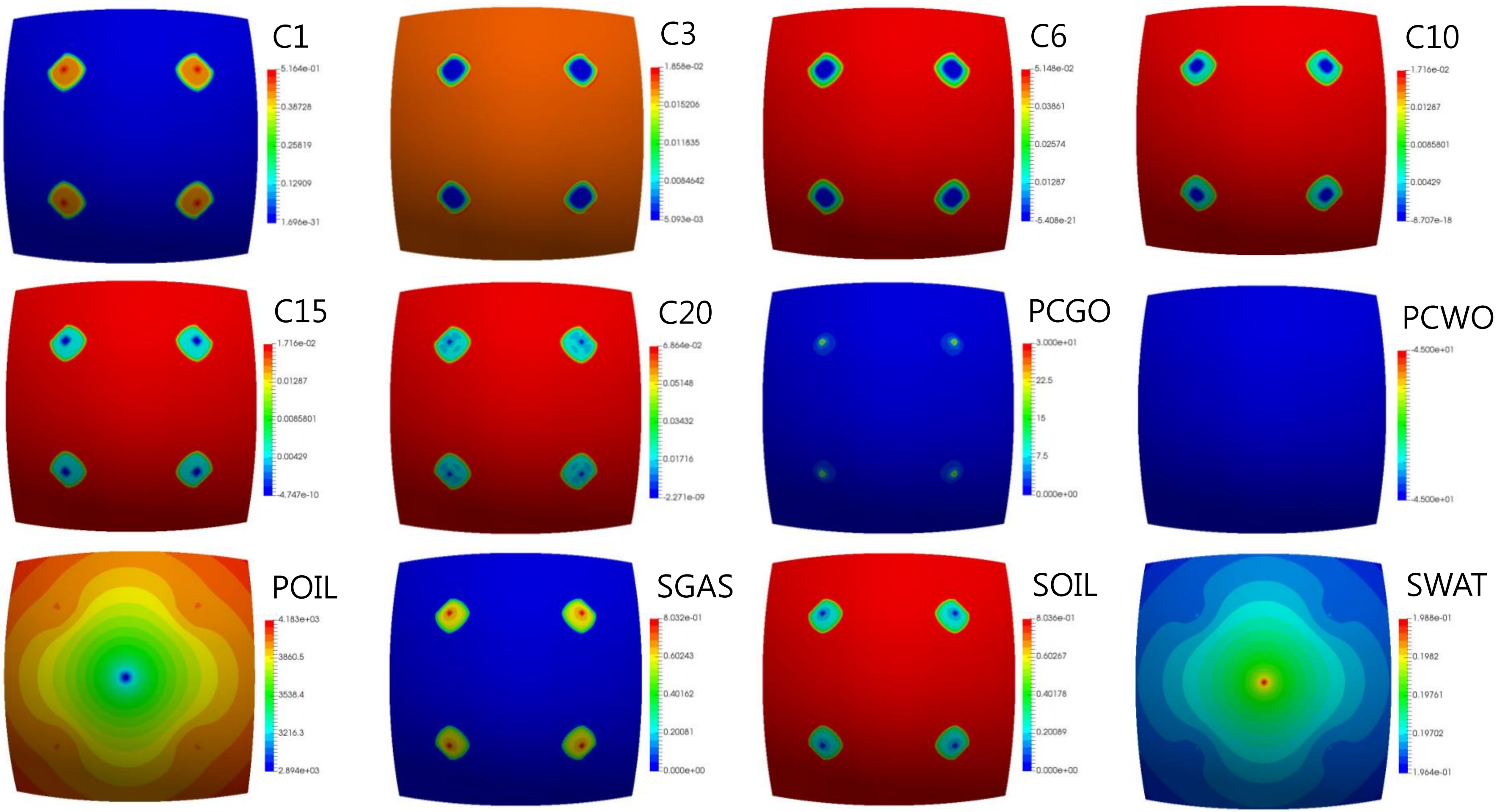

Ex: Runtimes and Speedup

Strong Scaling, Hard Phase Behavior

Runtimes

Procs.	Coeff.	Flash	Solve	Update	Total*
64	7510	404	3208	470	11530
128	3845	317	1993	262	6426
256	1956	105	1405	138	3616
512	1064	72	3404	68	4750
1024	592	36	1598	34	2460

Speedup normalized to 64 procs.

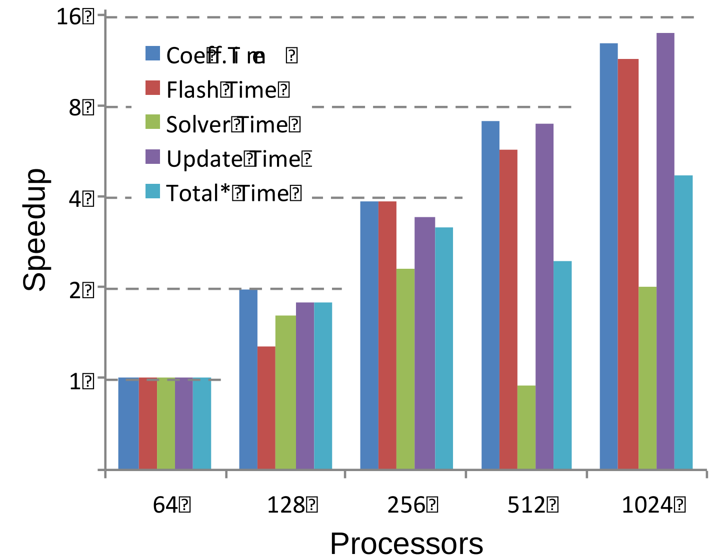

- Both coefficient assembly and updates scale optimally. Coefficient time twice as large as previous cases.
- Flash calculations order of magnitude more expensive, but still small fraction of total time. Scales better because not merely located by wells.
- Linear solver scales to 256 procs, and again decreases at 1024 procs.

Ex: Weak Scaling, Simple Phase Behavior

- Same simple phase behavior as Example 2, but with **weak scaling**. Need to keep problem characteristics the same on different levels.
  - Each processor owns 10,000 elements. Domain size increases with nu mber of processors.
  - Grid blocks remain 5x10x10 [ft^3], in order to keep same time steps.
  - Well locations are center of domain, and center of four quadrants.

Runtimes

Procs.	Elements	Coeff.	Flash	Solve	Update	Total*
64	640,000	295	14	255	17	576
256	2,560,000	176	9	342	10	550
1024	10,240,000	172	8	440	9	732

- Coeff, flash, and update improved from 64 to 256 procs, then remained const.
- Linear solver time increased slightly (note the problem is changing).
- Total time remains roughly constant, giving a positive weak scaling result.

Low-Tension Gas Flood Case Study: CoInj, WAG, SAG

Gas mobility control methods

- **Water Alternating Gas (WAG)**
- **Surfactant-alternate-gas (SAG)**
  - ➢ The 1st surfactant lowers Sor: reducing IFT
  - ➢ The 2nd surfactant controls gas mobility: generating foam
- **Simultaneous Water and Gas (CoInj)**

WAG

- Inject the 1st surfactant. Then, alternate water & gas

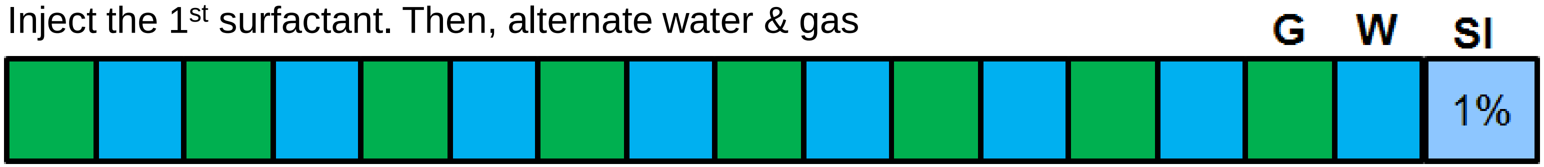

SAG

- Inject the 1st surfactant. Then, alternate 2nd surfactant foam & gas

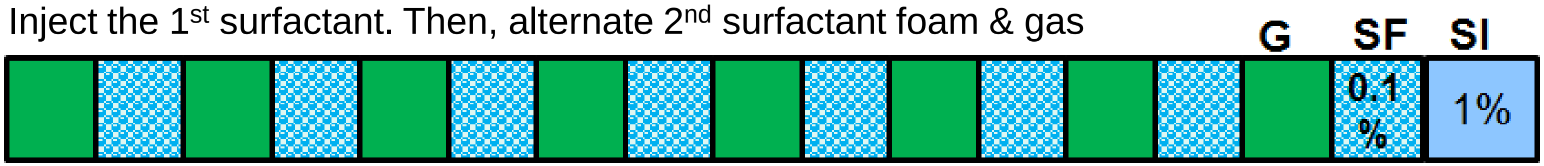

Co Inj

- SI: IFT-reduction surfactant; SF: Foam agent

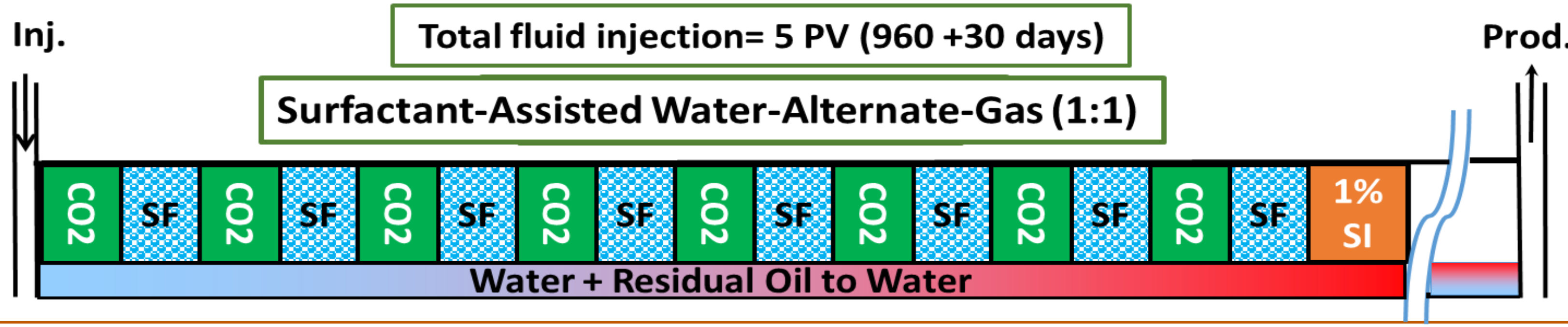

Low-Tension Gas Flood Case Study: CoInj, WAG, SAG

Model description

- $\Phi = 0.2;\ \frac{k_v}{k_h} = 0.1;\ S_o^{initial} = S_{orw} = 0.35$
- Initial pore volume = 53.4 MSTB
- $T^{initial} = 90°\text{F}\ ;\ P^{initial} = 1{,}500\ psia$
- Initial oil composition:

  C_{10}=30%; C_{15}=40%; C_{20}=30%
- Oil composition effect on ME phase behavior (2 set of parameters vs. EACN)

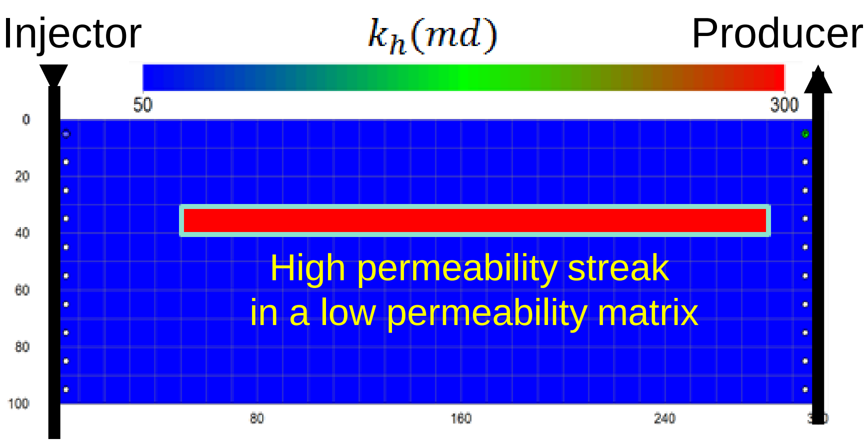

Simulation results

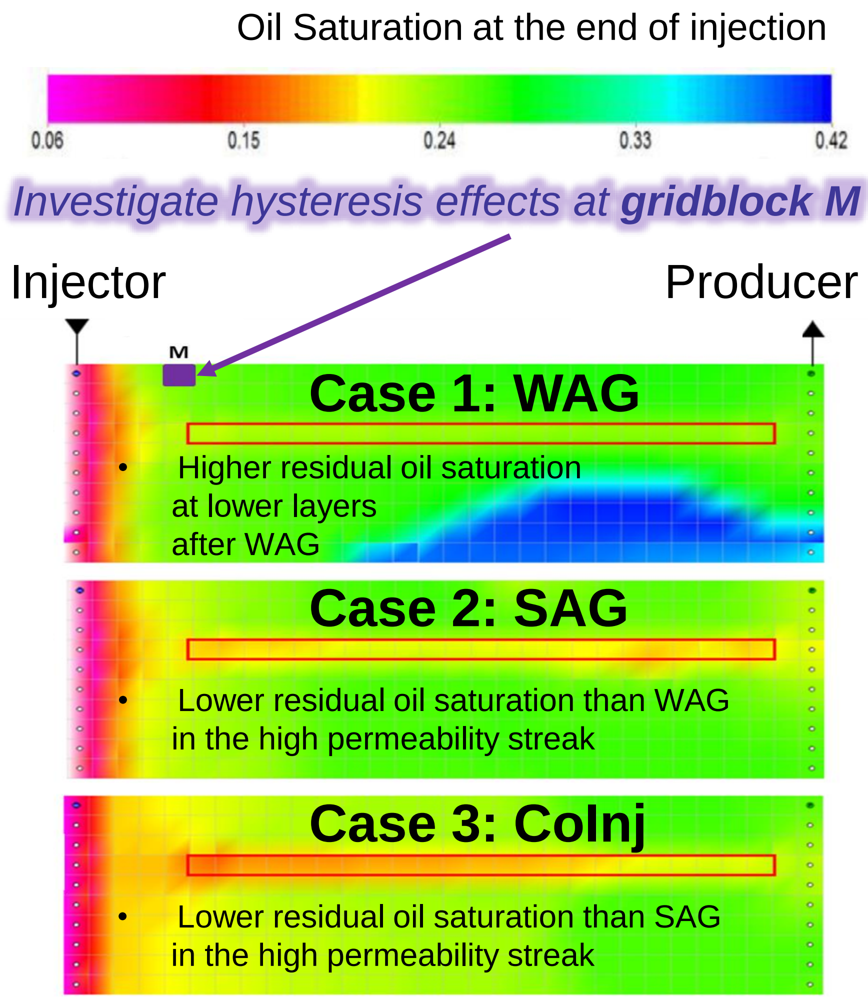

Low-Tension Gas Flood Case Study: K_{rg} and S_{gt} at the Gridblock M

Cycle-dependent relative permeability in multi-cycle WAG processes

- As the cycle number increases from the 1st to the 8th,
  - Gas relative permeability decreases in time.
  - Gas normalized trapped saturation increases monotonically.

  : due to hysteresis !

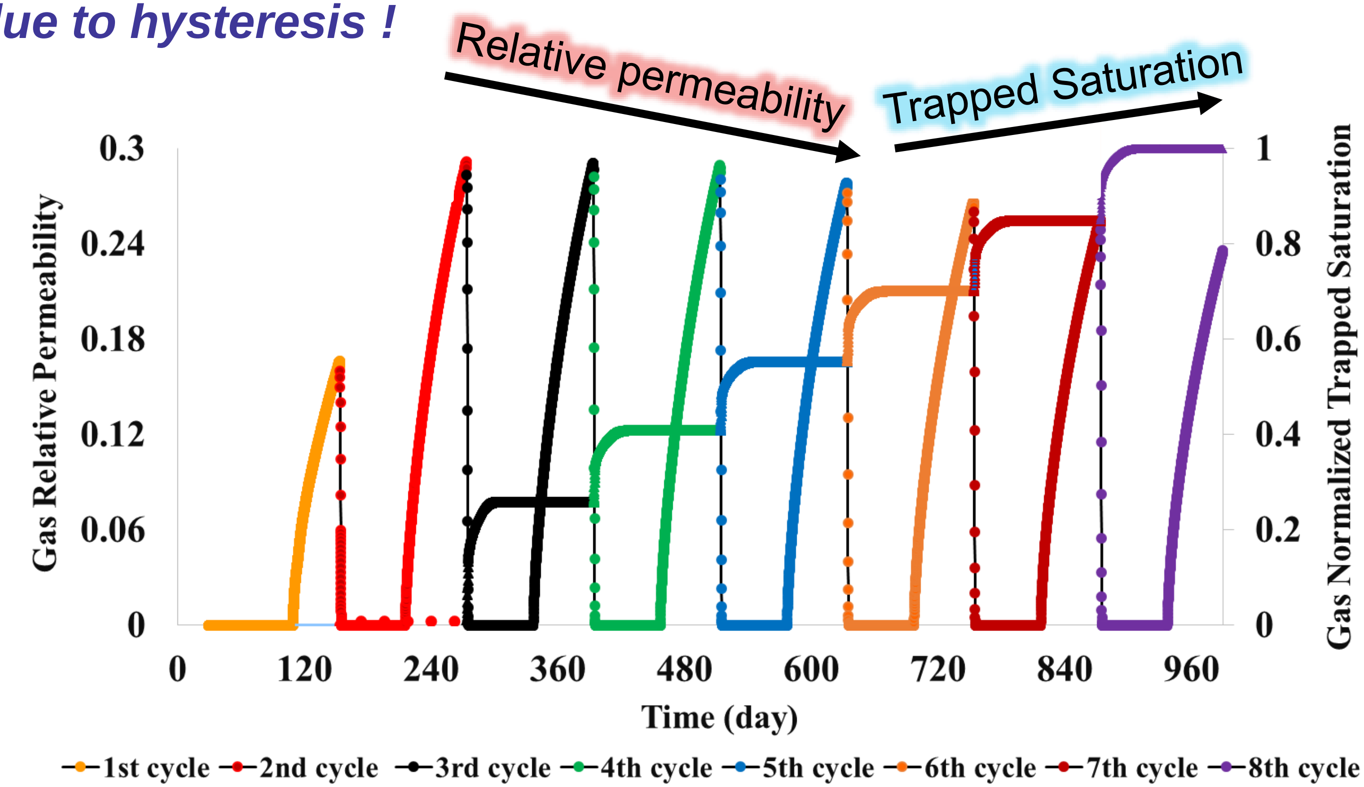

Effect of Water Alternating Gas (WAG) and Foam on CO_2 Sequestration

Introduction

- Three-phase relative permeability and hysteresis models are essential to accurately model CO_2 sequestration in aquifers.
- Once non-wetting phase saturation (here CO_2) decreases in porous media it traps by capillary forces (relative perm hysteresis, Beygi, 2016).
- Foam exhibits multiple steady-state behaviors at the same injection conditions (foam generation hysteresis, Lotfollahi *et al*., 2016).
- Three-phase relative permeability and hysteresis models have been implemented and coupled with foam models in IPARS.

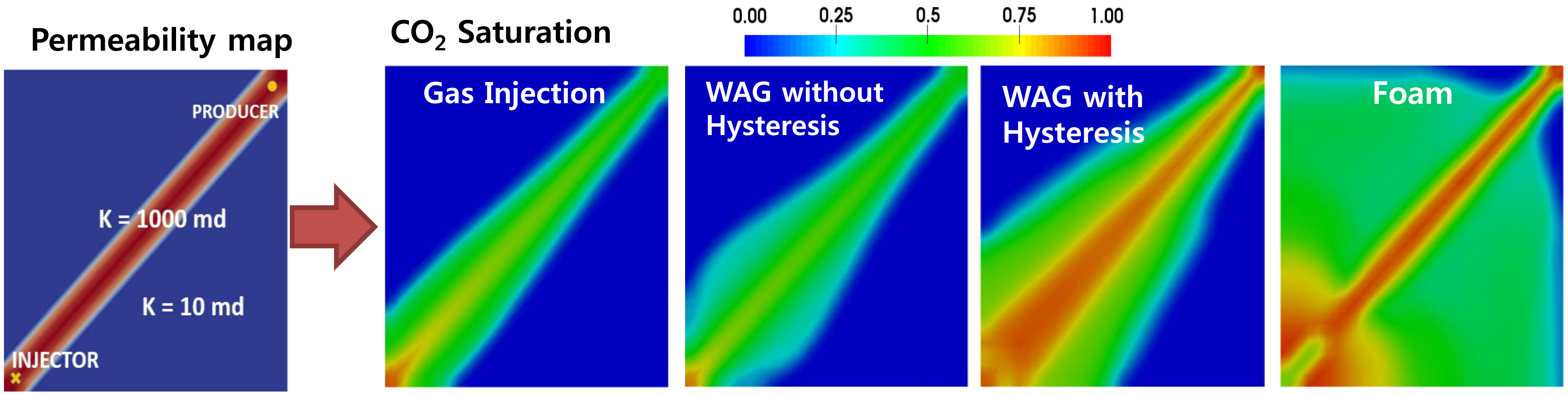

Effect of Water Alternating Gas (WAG) and Foam on CO_2 Sequestration

Findings

- Missing relative permeability hysteresis during WAG process underestimate WAG performance significantly.
- In surfactant alternating gas (Foam) process, strong foam is generated in the high permeability streak and divert the flow into low permeability matrix.

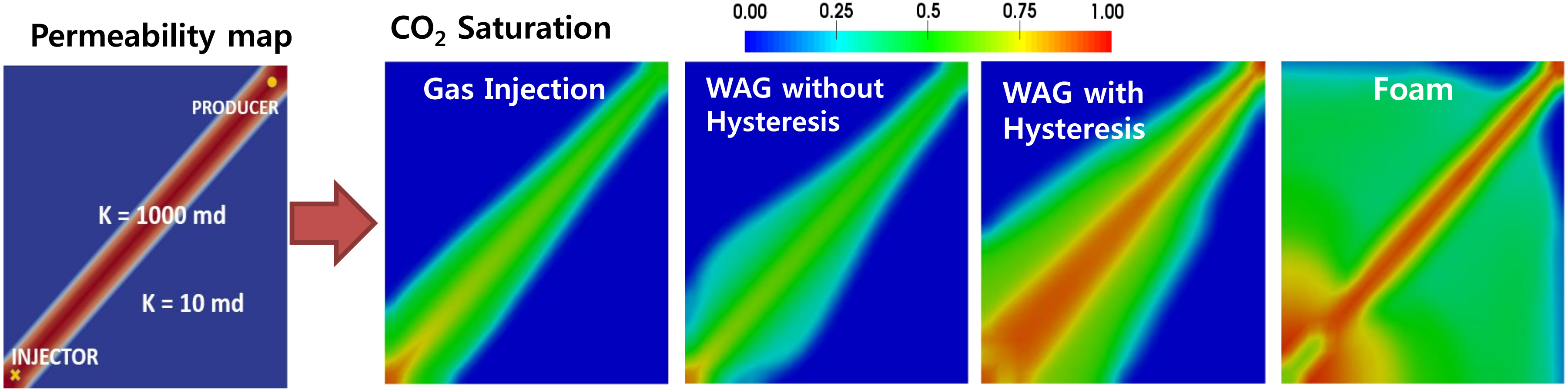

Poro-plasticitiy

- Geomechanical Effects of CO_2 Injection with a Poro-plasticity Model

Fluid Flow	$\frac{\partial(\rho(\phi_0+\alpha\varepsilon_v+\frac{1}{M}(p-p_0)))}{\partial t}+\nabla\cdot\left(\rho\frac{K}{\mu}(\nabla p-\rho g\nabla h)\right)-q=0$	
Stress Equilibrium	$\nabla\cdot(\sigma''+\sigma_o-\alpha(p-p_0)I)+f=0$	
Hooke's Law	$\sigma'' = D^e:(\varepsilon-\varepsilon^p)$	Druker-Prager Yield Surface
Strain-Displacement Relation	$\varepsilon = \frac{1}{2}(\nabla u+\nabla^T u)$	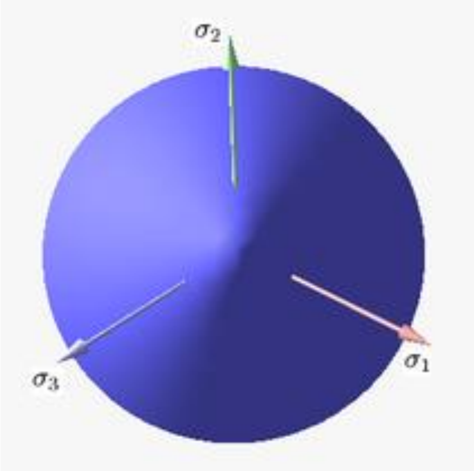
Plastic Strain Evolution	$\dot{\varepsilon}^p = \lambda\frac{\partial F(\sigma'')}{\partial\sigma''},\quad \text{at } Y(\sigma'')=0$ $\dot{\varepsilon}^p = 0,\quad \text{at } Y(\sigma'')<0$	
Yield and Flow Functions	$Y = q+\theta\sigma_m-\tau_0$ $F = q+\gamma\sigma_m-\tau_0$	

Model Field Sites

Objectives	Modeling, simulation & uncertainty analysis with application to CO_2 storage sites (Cranfield, MS & Frio, TX)

- Measure mechanical properties in laboratory
- Collect other existing data (seismic, well logs, etc.)
- Measure impact of geochemical alteration on mechanical properties
- Study rock dissolution and its effect on weakening the rocks and creating leakage pathways
- Enhanced simulation for studying and quantifying parameters, e.g. reservoir over pressure, chemical and thermal loading

Site 1: Cranfield, MS, USA

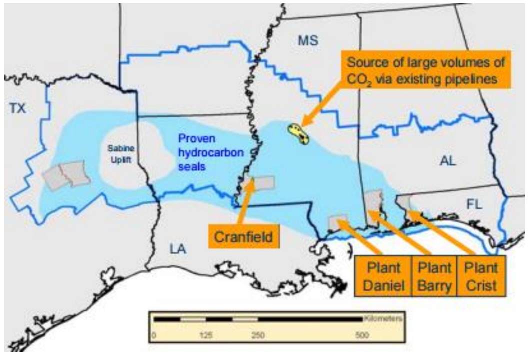

Site 2: Frio, TX, USA

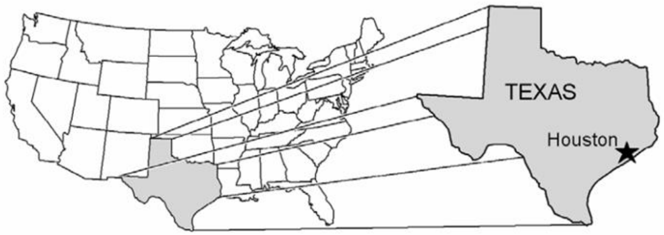

Example 2: Large-Scale Parallel Cranfield CO_2 Sequestration Case

CO_2 concentration on distorted grid

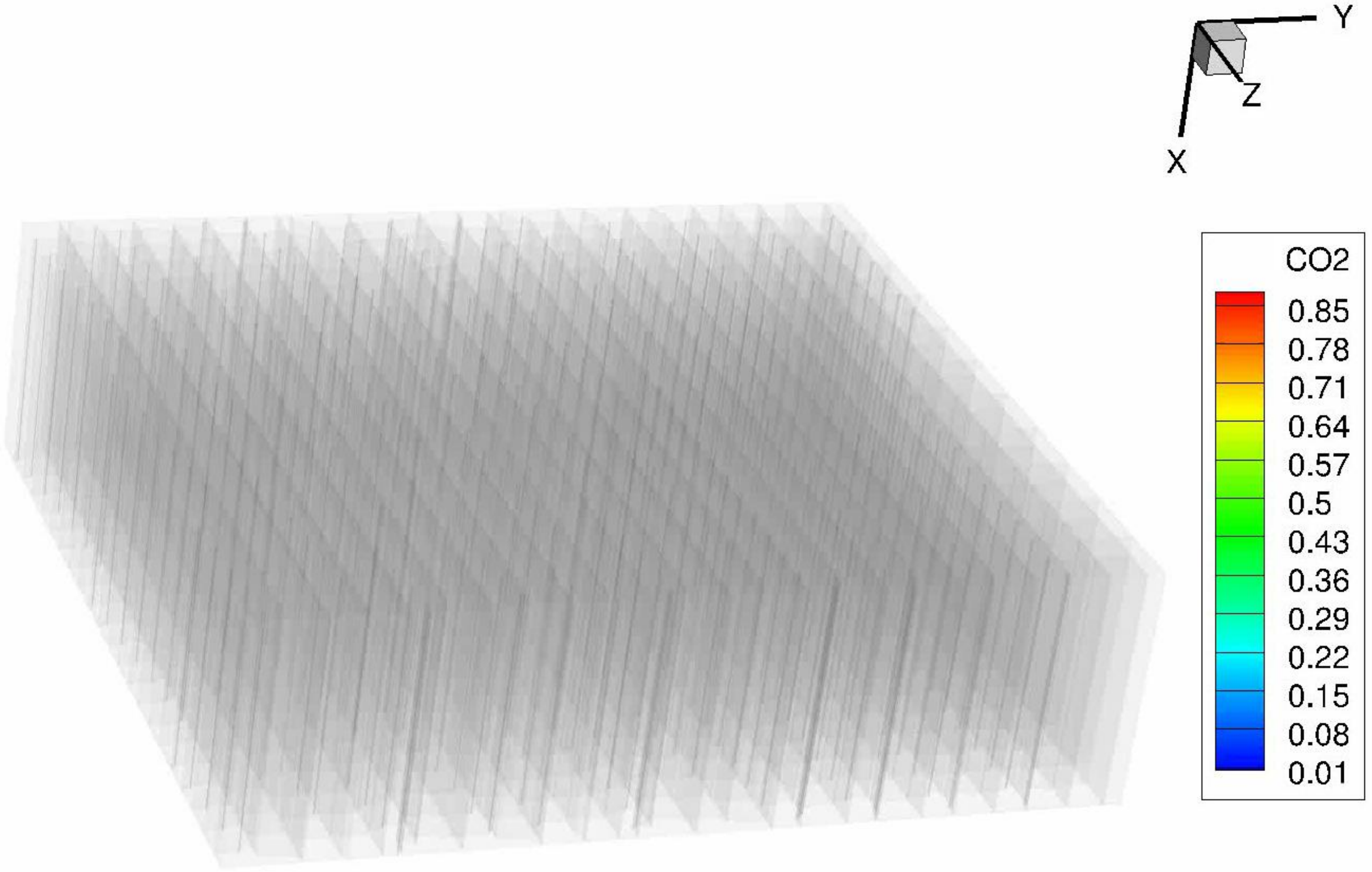

IV. UNCERTAINTY QUANTIFICATION

- Calibration process of rock and fluid properties in subsurface models

A Priori Model

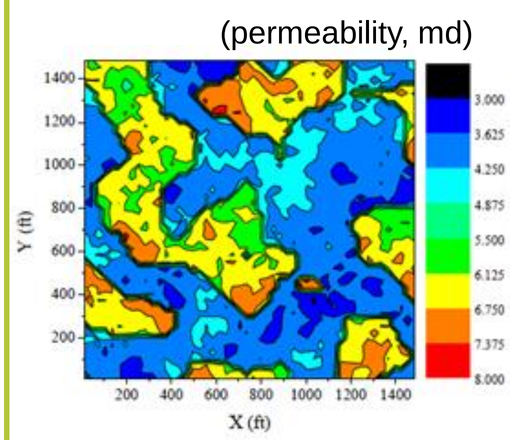

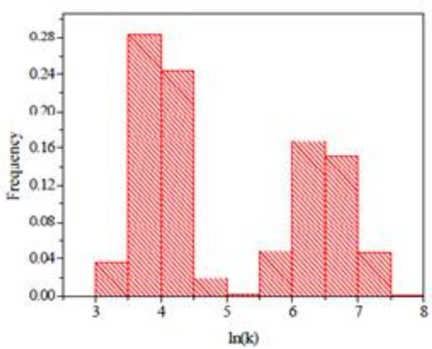

Multi-modal

History Matching

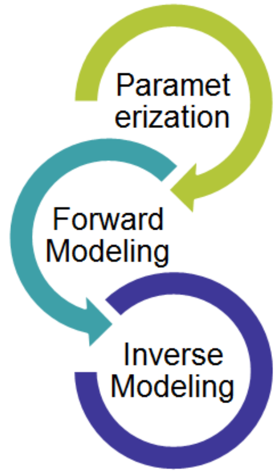

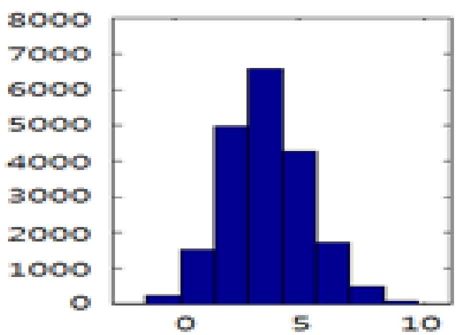

Gaussian

A Posteriori Model

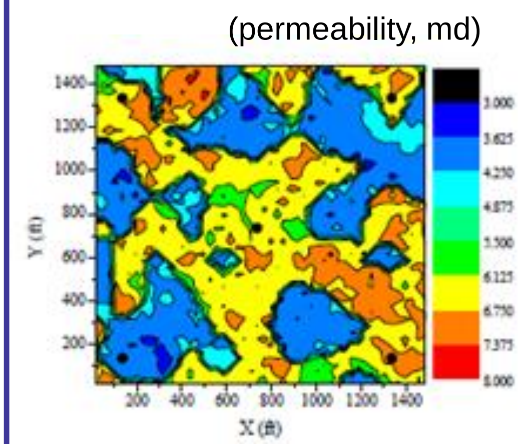

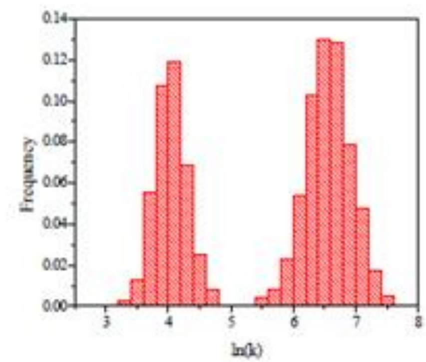

Multi-modal

Parallel Multi-objective Optimization for CCS at Cranfield

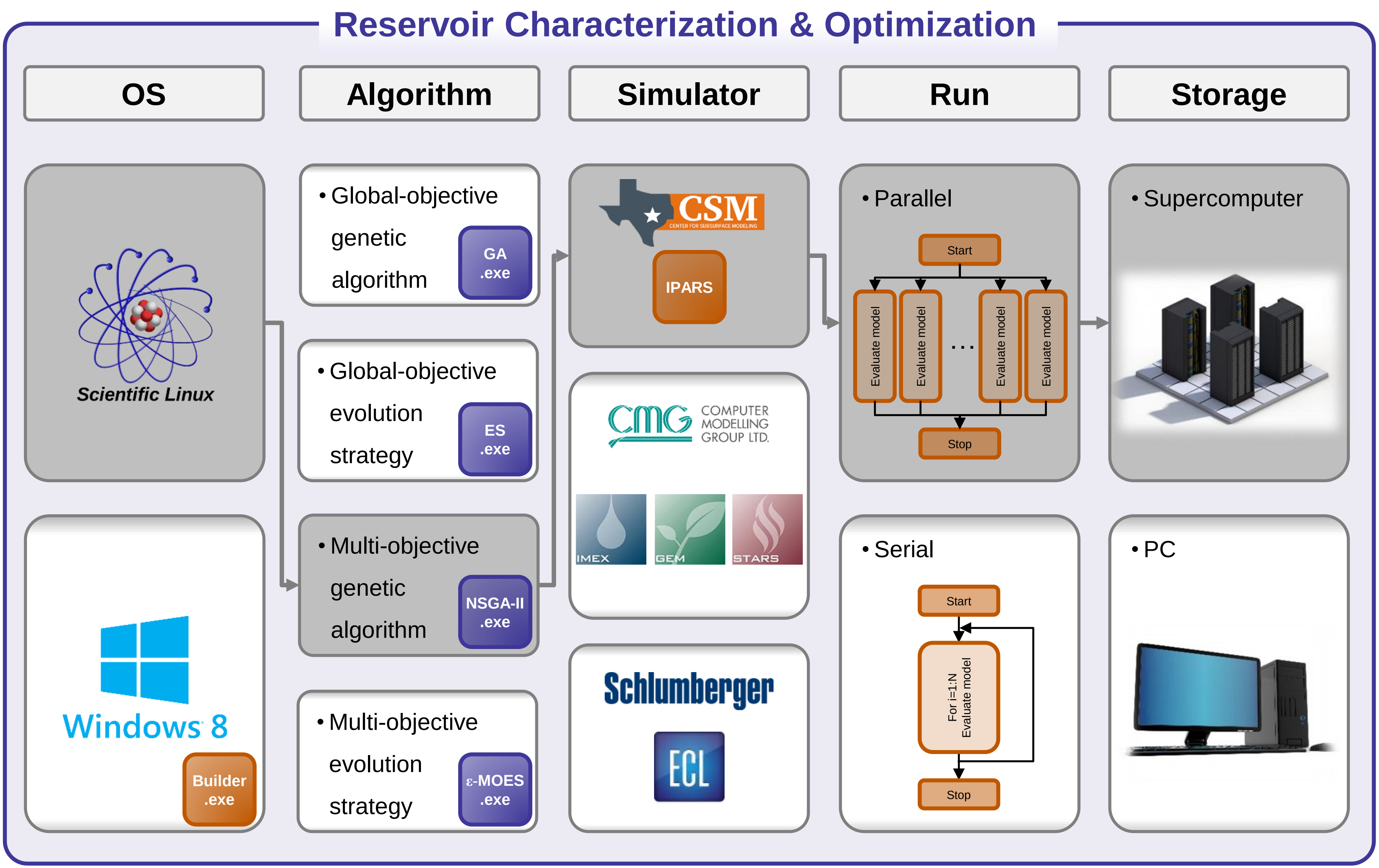

Modeling of CCS Site: Cranfield, Mississippi, USA

Numerical validation of pulse testing results

- Objective: validate pulse testing as an active monitoring tool for potential CO_2 leakage detection at geological carbon sequestration sites

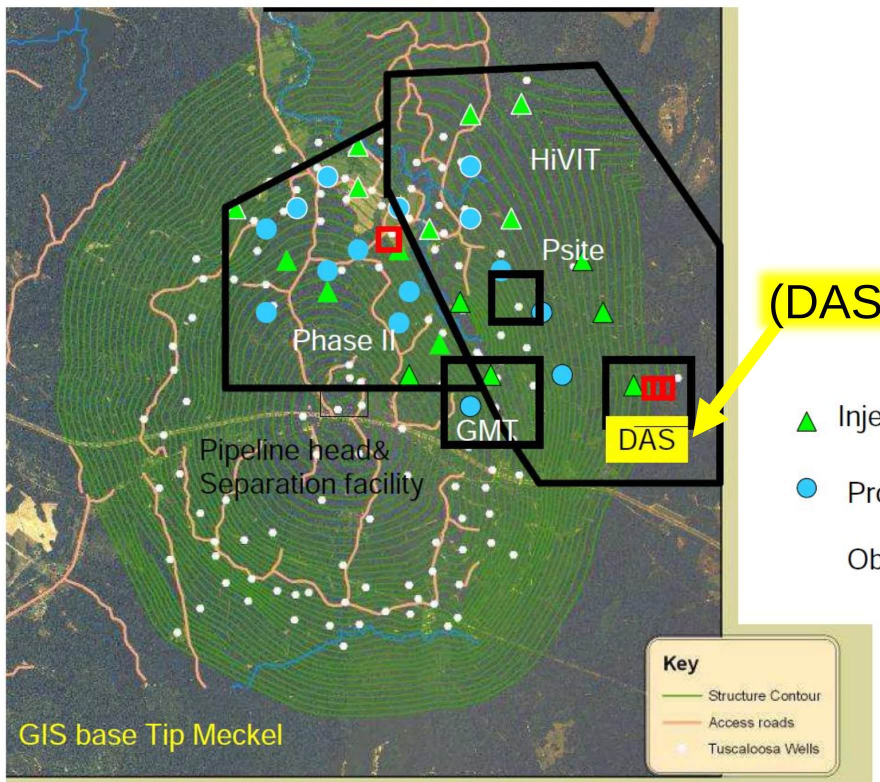

(DAS: detailed area of study)

Injector

Producer

Observation Well

(Lu et al., 2013)

Cranfield Sector Model

Three wells in the DAS (Detailed Area of Study) of Cranfield sector model

200 ft 100 ft

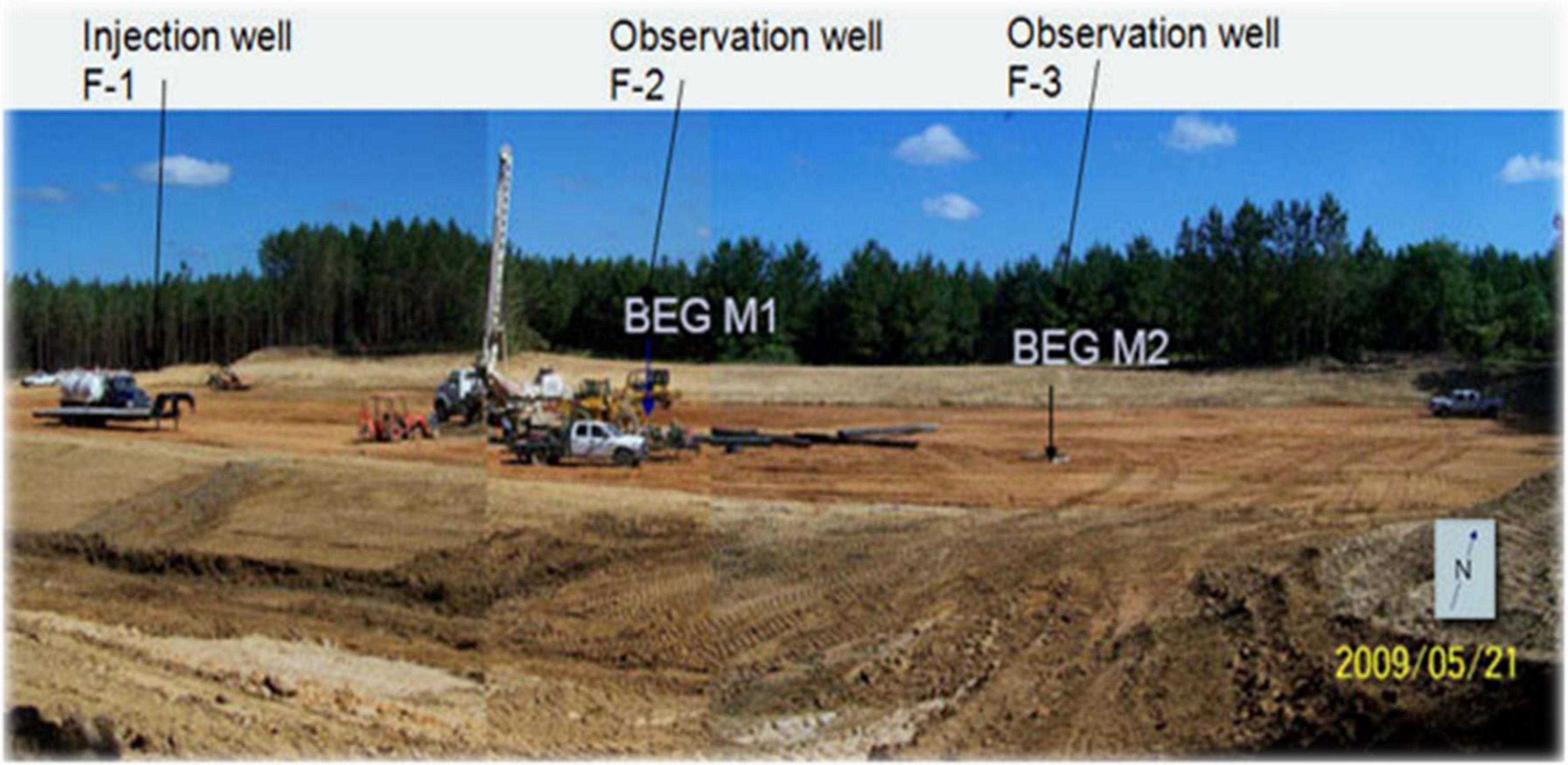

(http://www.beg.utexas.edu/gccc/cranfield.php)

Subsurface Modeling of Cranfield Sector Model

Grid top of Cranfield sector model

- 661,760 = 20x188x176 grid cells
- Grid size: 4 ft x 50 ft x 50 ft
- Side View

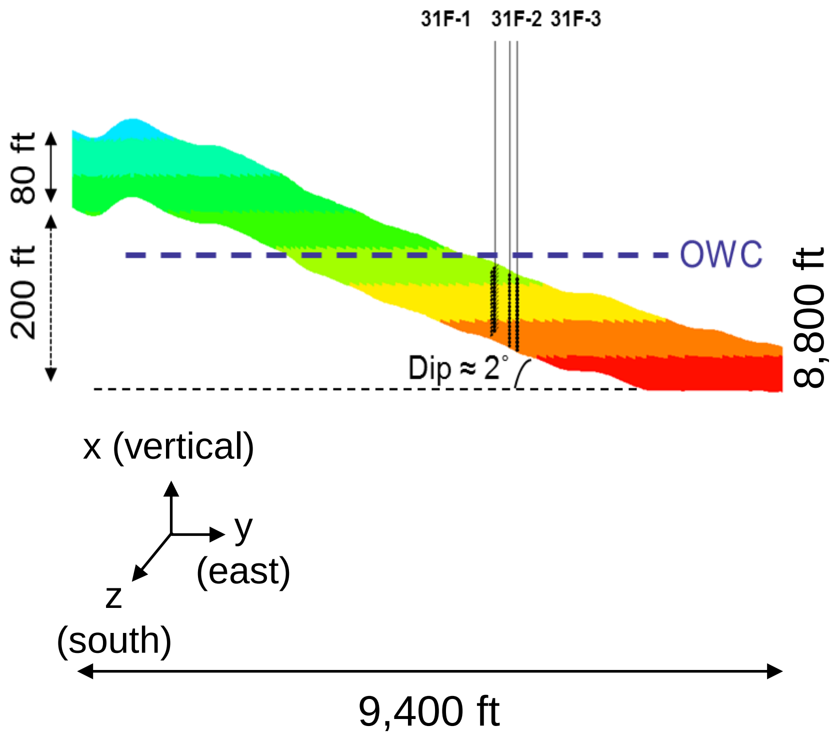

- Aerial View

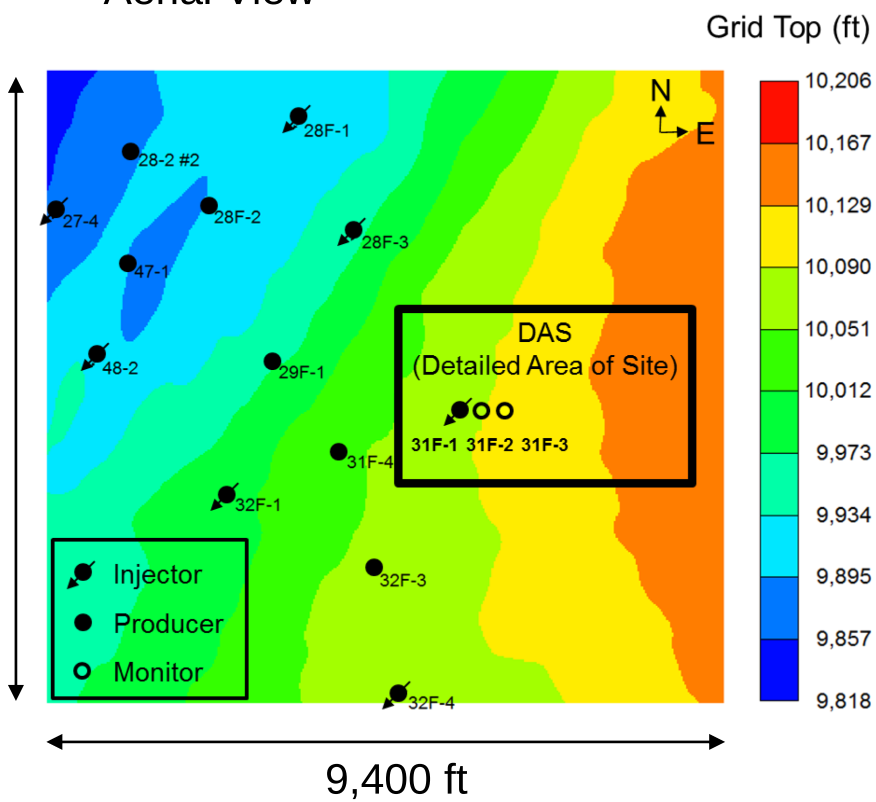

History Matching of Cranfield Sector Model

Bottomhole pressure at the CO_2 injection well 31F-1

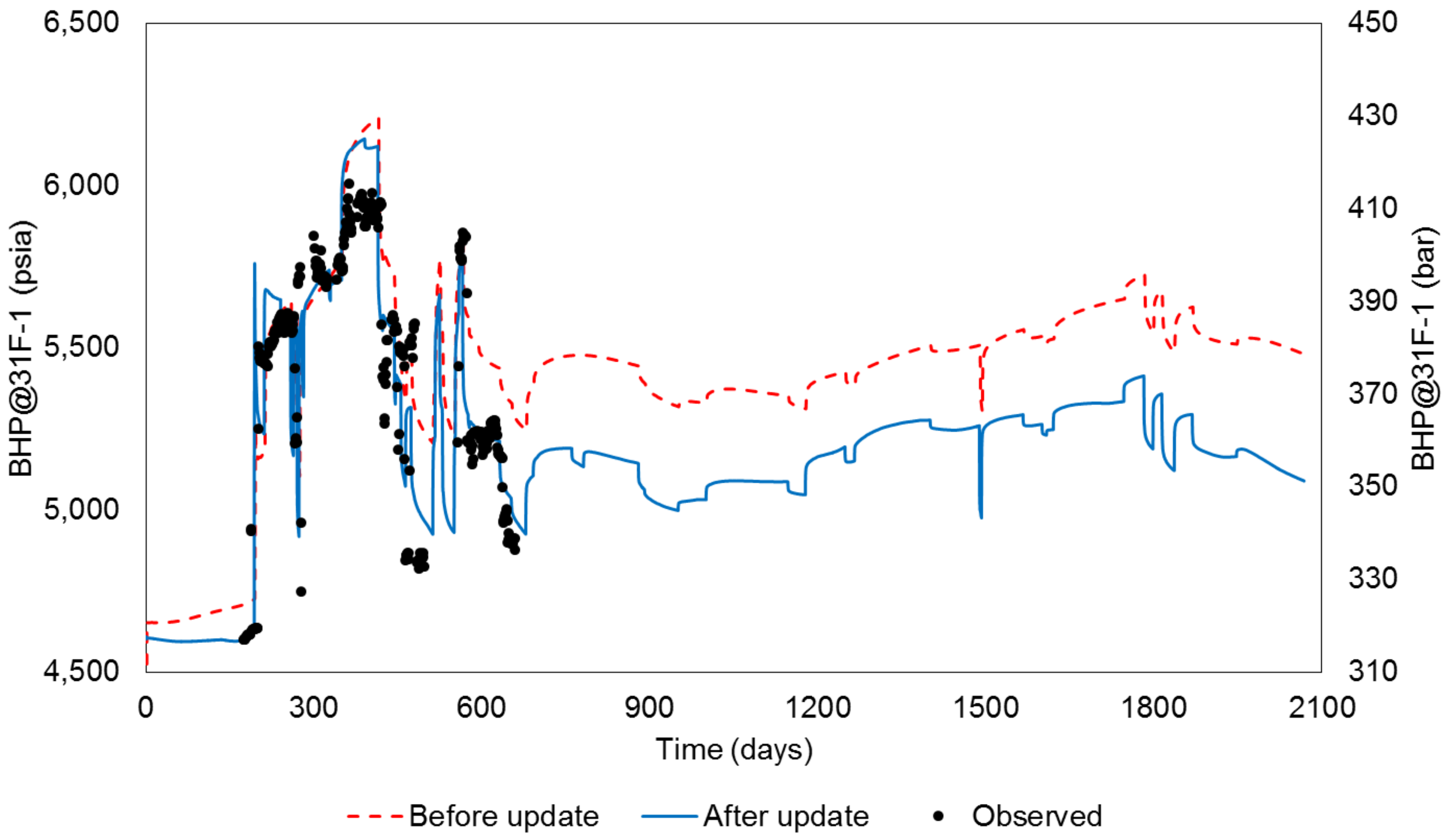

(Delshad et al. 2013) (Min et al. SPE-182641)

Compositional Simulations of Pulse Testing in the DAS

150-minute baseline experiment at the monitoring well 31F-2

- Observed pressure

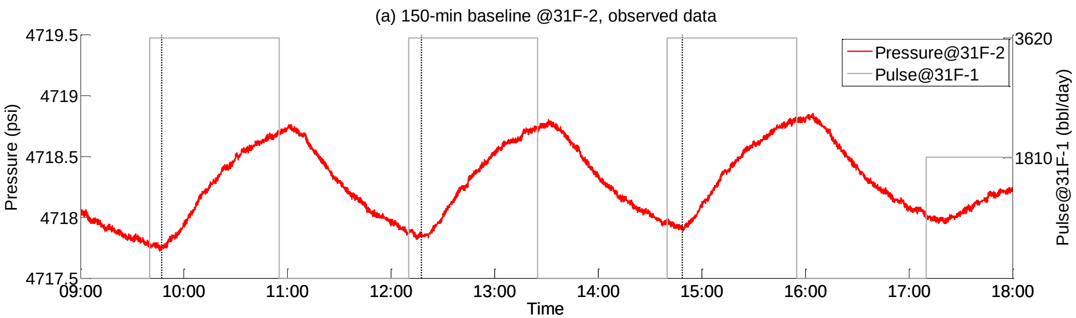

- Simulated pressure

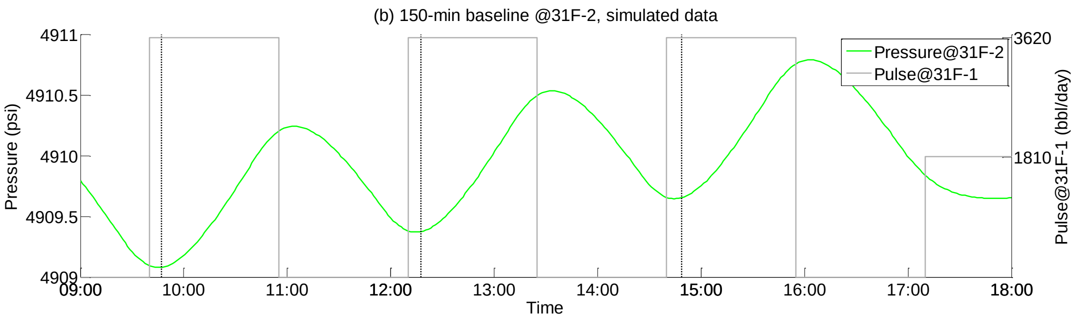

- Pressure anomalies obtained from observed & simulated pressure

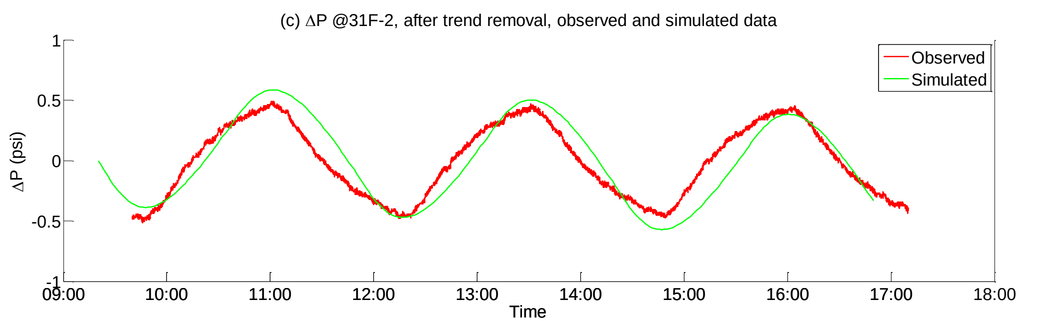

150-minute Baseline and Leak Experiments at Well 31F-2

Observation results

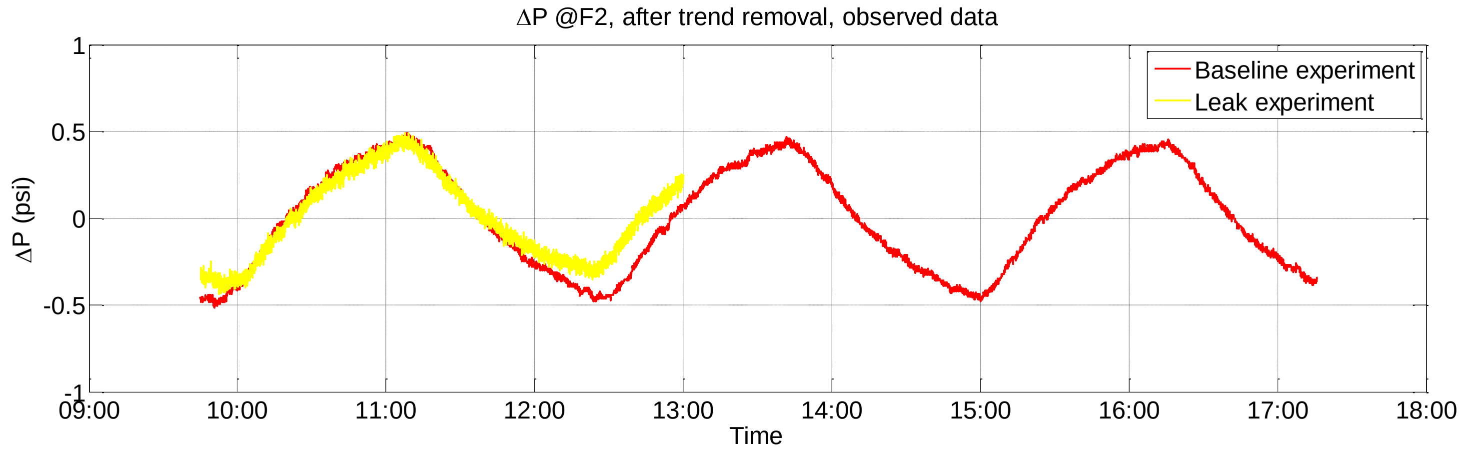

Simulation results

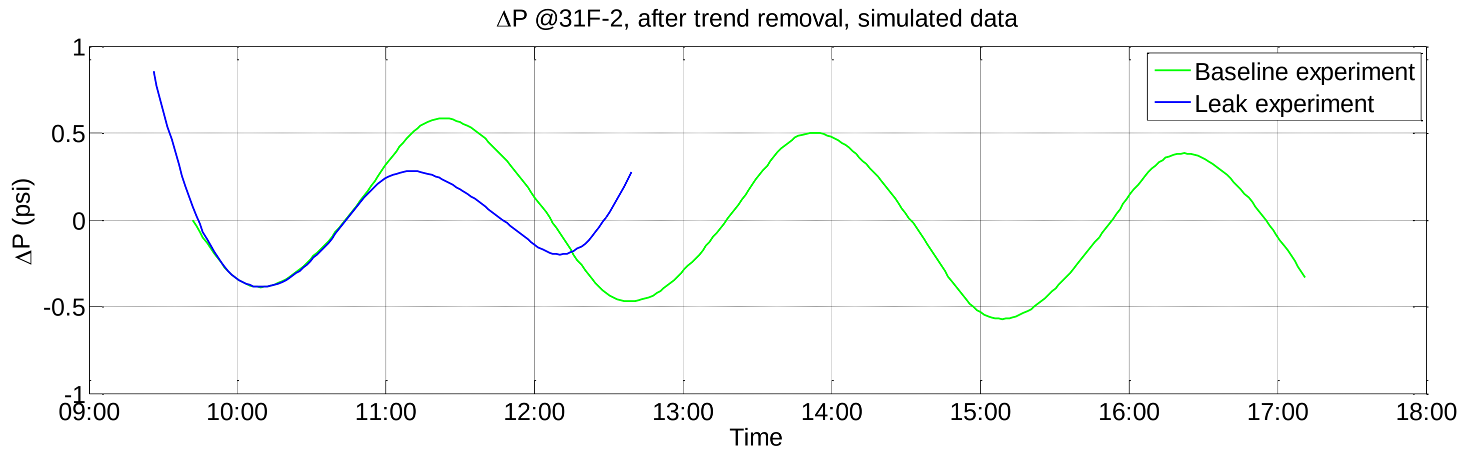

V. BIGDATA

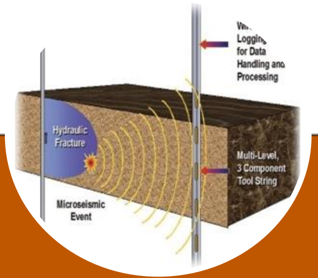

Characterization

- Computation of seismic wave propagation in fractured media
- Statistical (pattern recognition) schemes for identification of fracture characteristics from dynamic data

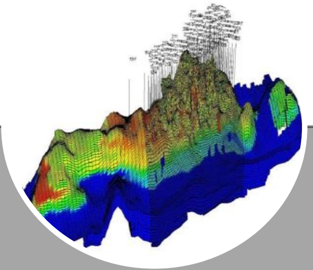

Simulation

- Large scale reservoir simulation of coupled compositional flow model and fracture propagation using Dataspaces
- Modeling of proppant filled fractures using Enhanced Galerkin

Optimization

- Optimized well spacing for hydraulic fracturing
- Multi-objective optimization process to choose geologic models based on observed flow and geomechanical responses

BIGDATA: Collaborative Research for Fractured Subsurface Characterization Using High Performance Computing and Guided by Big Data

❑ Data staging As-a-Service

Data staging enables coupling of multi-physics with big data

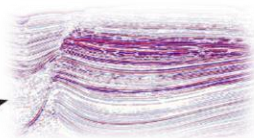

Seismic

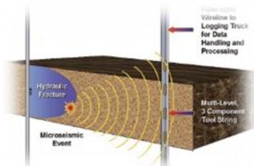

Microseismic

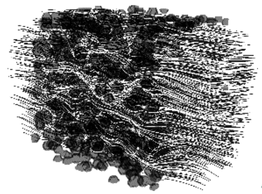

Flow

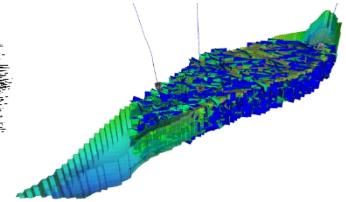

Fracture

InSAR

❑ Geophysics

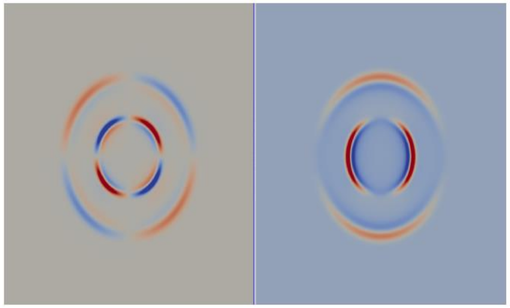

- Wave propagation

In fractured porous medium

❑ Reservoir Engineering

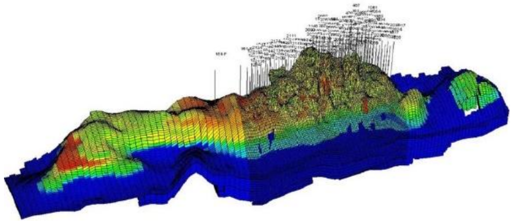

- Fracture propagation
- Data assimilation
- Production forecasts

❑ Big Data Analytics

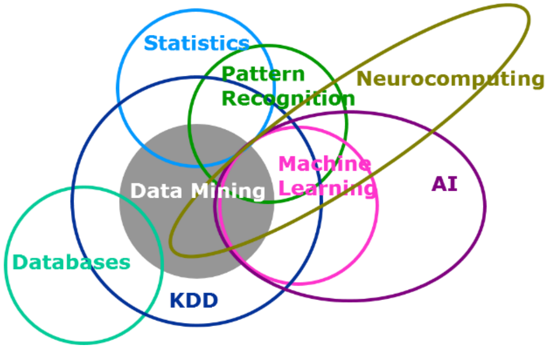

- Pattern recognition
- Deep neural network

Enriched Galerkin and Wave Propagation

❑ Phase Field and Seismic Wave Propagation in Fractured Media (Sen et al., 2017)

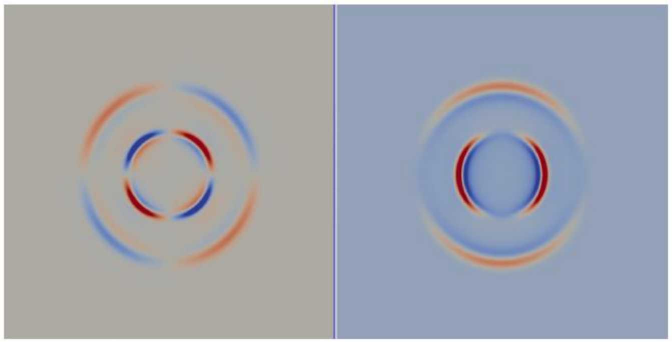

Wavefield using discrete fractures
540,384 Fractures – DG.

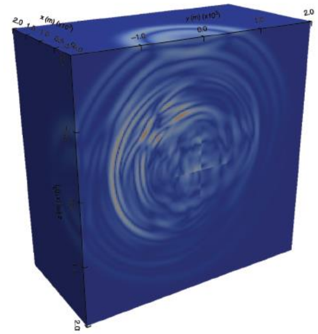

Orthogonal
fracture planes.

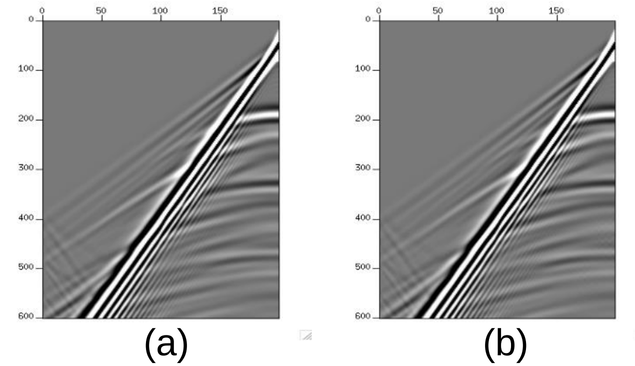

(a) Parallel to fracture
(b) Normal to fracture.

❑ Locally Conservative Finite Element Method

- ✓ Enriched Galerkin approximations for flow & transport
- ✓ Chemical reactions and viscous fingering
- ✓ Extended for seismic wave propagation

Viscous fingering in a two homogeneous channel.

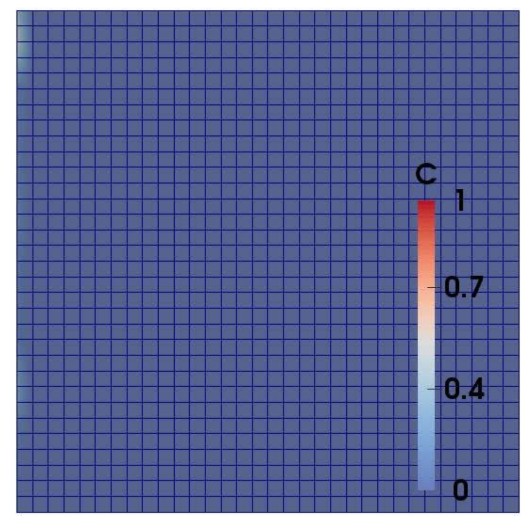

Dynamic mesh adaptivity.

Subsurface Fracture Characterization

❑ **Pattern Recognition for Fractured Reservoir Characterization Using Subsurface Big Data (led by Dr. Sanjay Srinivasan in Pennsylvania State University)**

✓ **Objective**

- Identify fracture location & orientation in low signal-to-noise ratio seismic data

✓ **Input training images**

- Seismic amplitude slices
- Fracture and non-fracture window examples

✓ **Validation data**

- Ku-Maloob-Zaap fields (Gulf of Mexico)
- 3D seismic
- Number of traces: 6,476,056
- Number of fractures: 1,000,000+

Penn State Initiative for Geostatistics & Geo-Modeling Applications

PennState

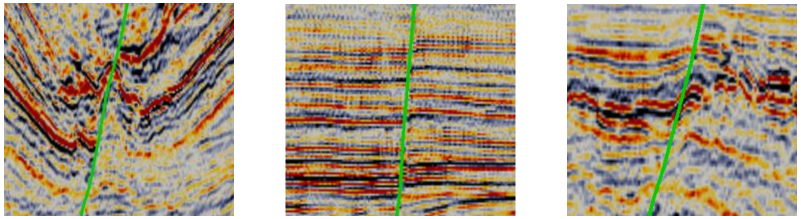

Sample positive training images

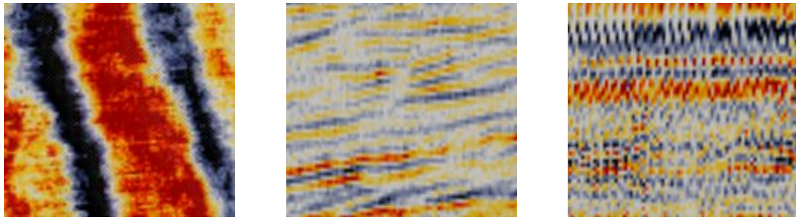

Sample negative (non-fracture) training images

Toolbox for Subsurface Big Data Analytics

- **Framework of a Computer-Assisted Optimization Toolbox: UT-OPT**

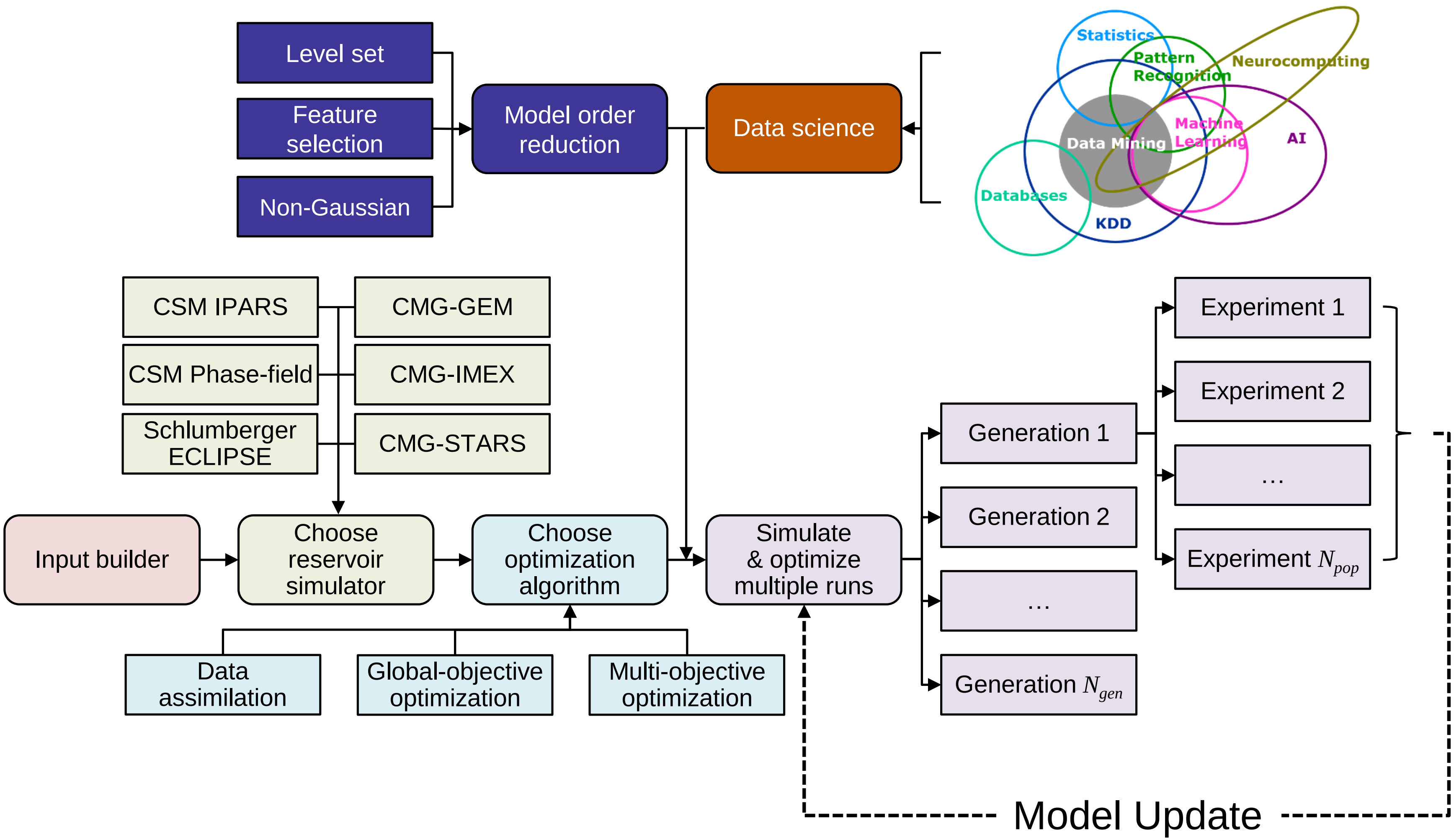

Framework of UT-OPT.

Workflow for Multiphysics Coupling of IPARS and deal.II using Dataspaces

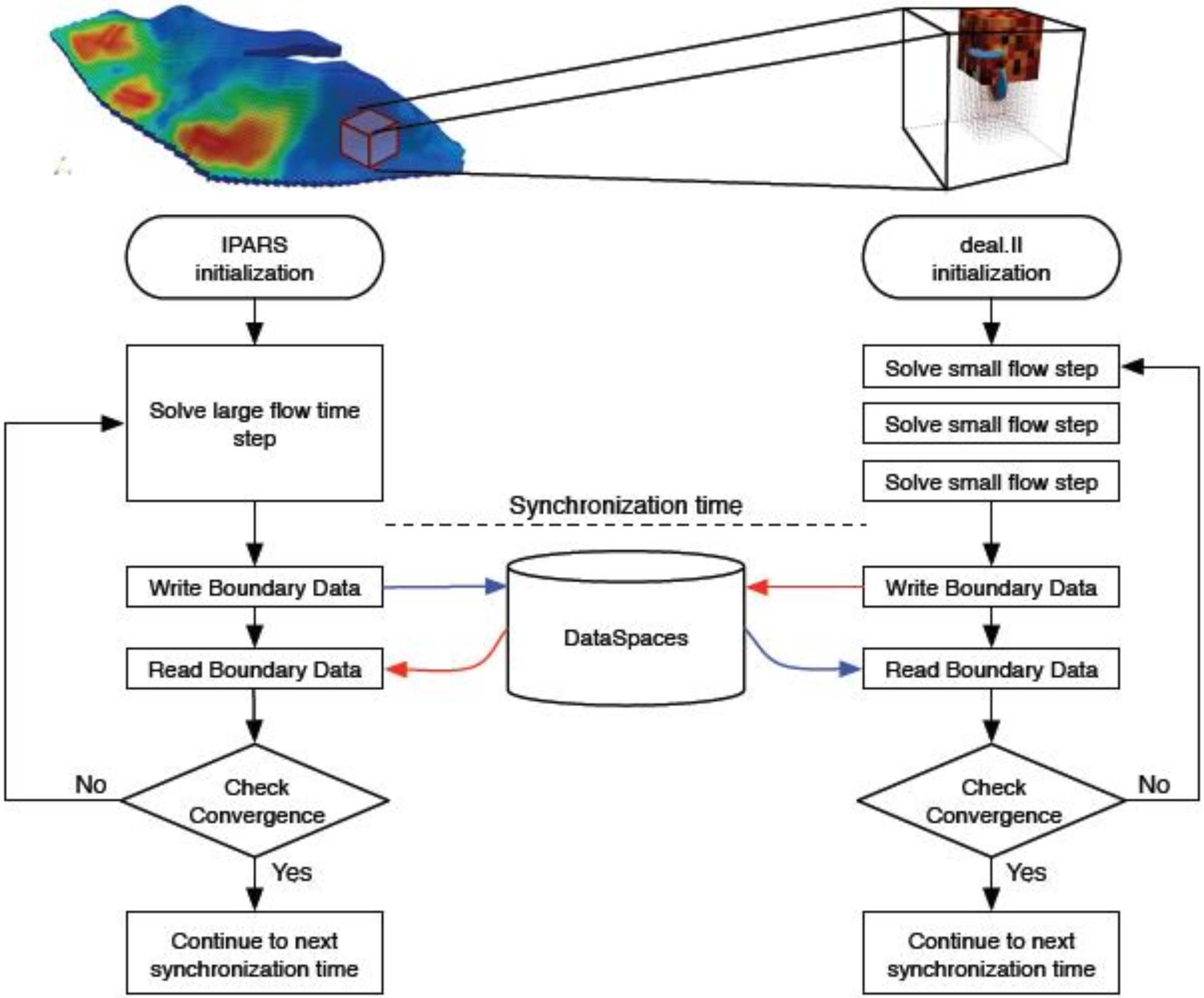

DataSpaces: Extreme Scale Data Management Framework for Data Staging

- **Key Features of Service-Oriented Staging**

  (led by Dr. Manish Parashar at Rutgers University)

RUTGERS
THE STATE UNIVERSITY OF NEW JERSEY

- ✓ **Dynamic:** coupled applications can join and leave staging areas without affecting other applications
- ✓ **Persistent:** The staging service and the staged data remains persistent across instances of the component applications. Applications can join and leave the staging service whenever they need access to it.
- ✓ **Efficient:** Optimizes the write perform ance by routing data from requesting client applications to the *closest* stag-ing servers
- ✓ **Resilient:** The staging service can be backed up and restarted as needed.

Exascale Computing

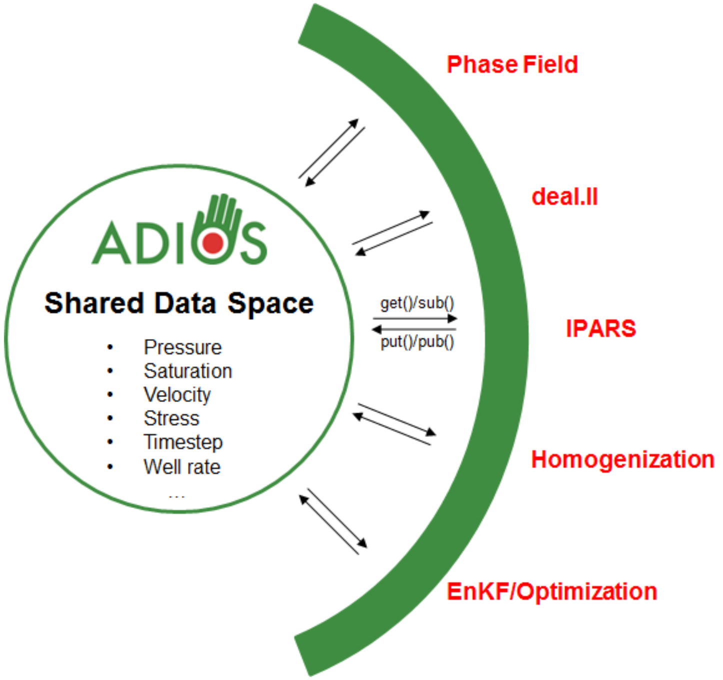

Shared data space ADIOS
that are to be coupled with forward models
and assimilation/optimization algorithms.

Coupled Compositional Flow Simulations with Fracture Propagation

Fluid Pressure

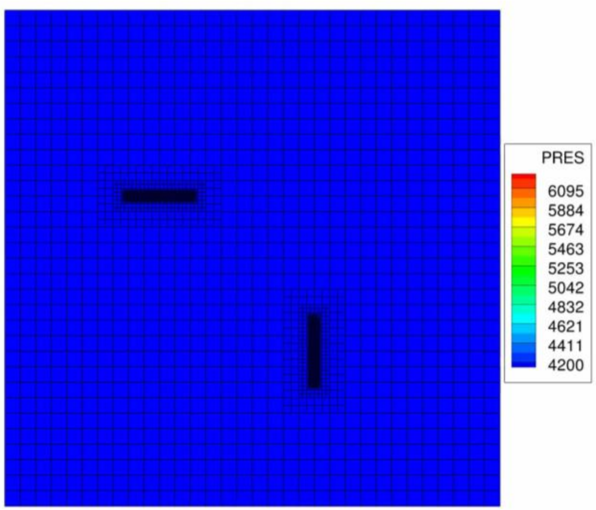

Water Saturation

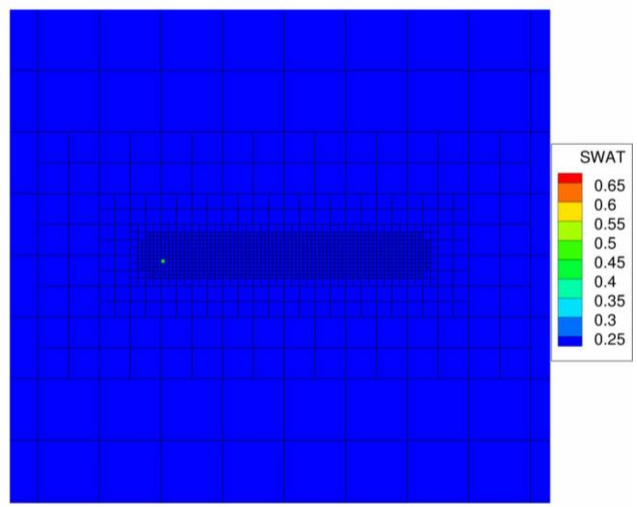

C6 Component Concentration

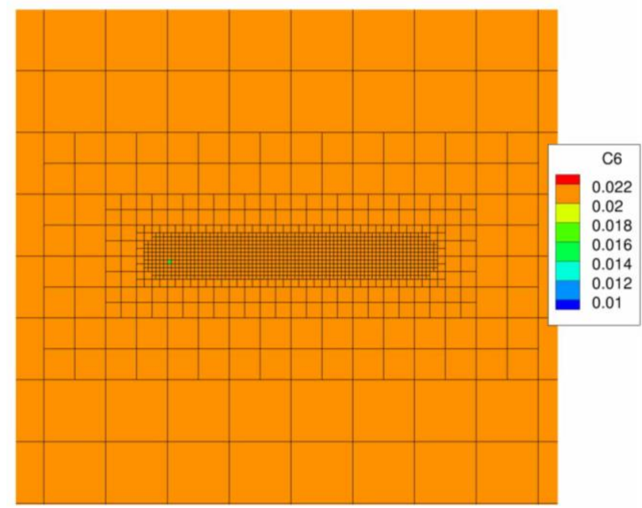

Conclusions

❑ Ongoing works: multidisciplinary collaboration with multi-universities, industry, government laboratories

- Part of training graduate students for future work force

❑ Big data: service-oriented data staging for coupling geophysics and flow with data

- Key features of data staging: dynamic, persistent, efficient, and resilient

❑ Development of high-fidelity algorithms: EG, Phase Field, Multipoint Flux, etc.

- Flow, transport, and mechanics in fractured porous media
- Wave propagation
- Data assimilation & multiobjective optimization
- Machine learning & pattern recognition